Investigation of the Oxidative Activity of Giardia Flavohemoglobins

A thesis submitted to the Committee on Graduate Studies in partial fulfillment of the requirements for the degree of Master of Science in the Faculty of Arts and Science

Trent University

Peterborough, Ontario, Canada

Environmental and Life Sciences M.Sc. Graduate Program

April 2025

ABSTRACT

Investigation of the Oxidative Activity of Giardia Flavohemoglobins

Isabelle Decorso

Flavohemoglobins are enzymes primarily implicated in nitrosative stress due to their high nitric oxide (NO) dioxygenase activity and transcriptional upregulation in response to NO. *Giardia intestinalis* assemblages A, B, and E possess flavohemoglobins (gFlHb) that may function beyond their NO dioxygenase activity, potentially contributing to oxidative stress regulation, as transcriptional profiling revealed that peroxide also induces gFlHb expression. This study investigates gFlHb's NADH oxidase activity in the absence of NO, structural interactions with lipids, and response to reactive oxygen species. Minor differences in NADH oxidase activity among assemblages were observed, and their susceptibilities to inhibition were assessed to evaluate gFlHb as a potential therapeutic target against Giardia infection. Under aerobic conditions, we observed that gFlHb generates hydrogen peroxide, a surprising finding suggesting a self-regulating feedback mechanism involving reactive oxygen species and heme degradation. These findings provide new insight into the role of flavohemoglobins in microaerotolerant parasites like Giardia.

Keywords: *Giardia intestinalis*, heme, flavohemoglobin, lipids, NADH, oxidative stress, hydrogen peroxide

ACKNOWLEDGEMENTS

First and foremost, I would like to express my deepest gratitude to my supervisor, Dr. Steven Rafferty. Steve, I am extremely grateful for the opportunities and knowledge you have shared with me with over the past three years. What began as me forgetting to apply for a fourth-year thesis project, and you procrastinating selecting students, has evolved into an amazing mentorship. You created an engaging and supportive lab environment, always encouraging us to explore even the most outlandish ideas. It is because of you that I love research and that my academic journey is continuing in Montreal. Thank you.

I would also like to thank Dr. Janet Yee, who is a scientist I deeply admire. Janet, your accomplishments are truly inspiring, and I am grateful for the guidance and advice you have given me throughout my degree. I must also thank my supervisory committee, Dr. Craig Brunetti and Dr. Sanela Martic. Your expertise in areas beyond my own has been invaluable, and I deeply appreciate your support. As well, Naomi Scott who spent many hours running samples and assisting me with the mass spec.

I am incredibly grateful for the support and friendships I found within the Chemistry department. Dr. Eric Keske, Dr. Emily Slepkov, Dr. Jayme Stabler, Dr. Jen Hendel, Cassie DeFrancesco, and Teresa Garvey, your guidance and stories have made my time at Trent an overwhelmingly positive experience. I appreciate all the advice you shared, the conversations we had, and the reference letters you wrote for me. Additionally, being a TA was one of my greatest joys throughout my undergrad and M.Sc. To all my students, thank you for the laughter and energy that made teaching you so fulfilling. I was moved by your kind words and look forward to hearing how your journeys play out. Joel-Anthony and Nick, I could not have asked for better TA partners this year.

To the Rafferty and Yee lab groups, thank you for making the lab brighter, especially Sarah Hill, Melanie Marlow, and Logan Findlay. Sarah, you have been there through every lab high and low, and I cherish our friendship, as well as our *daily* Chicken Soup for the Soul passages. Mel, you are the easiest person to get along with, celebrate with, and complain with when experiments go awry. And Logan, collaborating with you has been epic, you keep me on your toes even when I'd rather not be. Best lab partner ever!

To Trevor, Carolina, Brooklyn, Mikaella, Bradley, and Mitch. I have found some of my best friends in all of you and I have the deepest respect and love for you. Spending countless hours playing games at The Only, playing games in Muskoka, playing games in our homes, playing games in Dougie, playing games at Trent, and playing games literally anywhere else have been some of my best memories. To my friends Kolby, Emma, Curtis, Rachelle, Kurtis, Kimmy, Beck, Gracie, and Draeden, I love you all dearly.

Finally, and most importantly, I would like to thank my family, my biggest and most unwavering supporters. Mom and Dad, none of what I have accomplished would have been possible without your love and support. You never gave me any idea that I couldn't do whatever I wanted to do or be whomever I wanted to be. Your emotional (& financial) support was never lost on me. Jessica, you are my best friend, and though I am older and usually wiser, I will always look up to you, your strength and resilience amaze me. Zach, your ability to travel for years on end and yet return as if no time has passed shows the bond our family has. To Nonna and Nonno, my Zias, Zios, and cousins, being away from home for the past six years has been one of my greatest challenges, but knowing you are always there makes it infinitely easier. My Decorso and Porcellato families are my ultimate inspiration for everything I do, thank you.

TABLE OF CONTENTS

LIST OF FIGURES

LIST OF TABLES

LIST OF ABBREVIATIONS AND SYMBOLS

ABZ	Albendazole
ALA	5-Aminolevulinic Acid
ANOVA	Analysis of Variance
CHT	Ceramic hydroxyapatite
cyt. *c*	Ferricytochrome *c*
DNA	Deoxyribonucleic Acid
e^-	Electron
ε	Extinction coefficient
FAD	Flavin Adenine Dinucleotide
Fe^{2+}	Reduced, ferrous iron
Fe^{3+}	Oxidized, ferric iron
Fe^{3+}- $O_2^{\bullet-}$	Ferric-Superoxide complex
FHP	*Alcaligenes eutrophus* flavohemoglobin
FMN	Flavin Mononucleotide
FNR	Ferredoxin $NADP^+$ Reductase
FPLC	Fast Protein Liquid Chromatography
ESI-FTMS	Electrospray Ionization Fourier Transform Mass Spectrometry
gFlHb	*Giardia intestinalis* Flavohemoglobin
GSH	Glutathione, reduced
GSSG	Glutathione disulfide, oxidized
H^+	Hydrogen ion
H_2O	Water
H_2O_2	Hydrogen peroxide
Hmp	*Escherichia coli* flavohemoglobin (Heme-like Protein)
HRP	Horseradish Peroxidase
IMZ	Imidazole
IQR	Interquartile Range
kDa	Kilodalton
LB	Luria-Bertani

μ	Micro
m	Milli
MCZ	Miconazole
mmHg	Millimeter Mercury
MTZ	Metronidazole
NAD^+	Nicotinamide Adenine Dinucleotide
NADH	Reduced Nicotinamide Adenine Dinucleotide
$NADP^+$	Nicotinamide Adenine Dinucleotide Phosphate
NADPH	Reduced Nicotinamide Adenine Dinucleotide Phosphate
Ni-NTA	Nickel-Nitrilotriacetic Acid
nm	Nanometers
$^{\bullet}NO$	Nitric oxide
NO_3^-	Nitrate
NOS	Nitric oxide synthase
O_2	Molecular oxygen
$O_2^{\bullet-}$	Superoxide anion
ODA	O-Dianisidine
$^{\bullet}OH$	Hydroxyl radical
PCR	Polymerase Chain Reaction
RNS	Reactive Nitrogen Species
ROS	Reactive Oxygen Species
rpm	Revolutions Per Minute
rRNA	Ribosomal Ribonucleic Acid
SDS-PAGE	Sodium Dodecyl Sulphate Polyacrylamide Gel Electrophoresis
SOC	Super Optimal medium with Catabolic repressor
SOD	Superoxide dismutase
SOR	Superoxide Reductase
TLC	Thin Layer Chromatography
UV	Ultraviolet

1. INTRODUCTION

1.1. Giardia intestinalis

Giardia intestinalis is a fascinating protozoan parasite that thrives in a low-oxygen environment and exhibits unique morphological features. As one of the most prevalent intestinal parasites affecting both humans and animals globally, Giardia has attracted considerable scientific interest in both research and clinical settings.[1] Giardia's life cycle includes a resistant cyst stage and a motile trophozoite stage that colonizes the host's gastrointestinal tract.[2] A comprehensive understanding of its biology and adaptation mechanisms are essential for developing effective interventions against giardiasis.

1.1.1. The global burden of giardiasis

Giardiasis, the intestinal disease caused by Giardia, presents a major health challenge worldwide. Intestinal protozoan infections, including giardiasis, are the second leading cause of morbidity and mortality,[1] with nearly 1.7 billion diarrheal cases reported annually.[3] Giardia is the most frequently identified parasite among these infections, contributing to at least 280 million cases each year and approximately 2.5 million deaths.[1] While giardiasis can often be asymptomatic and remain undetected, especially in developed regions, it may present with a range of symptoms, including diarrhea, nausea, vomiting, dehydration, and malnutrition. These symptoms typically emerge 1-2 weeks post-infection and can persist for 2-6 weeks.[4]

Transmission primarily occurs through the fecal-oral route, with contaminated food and water being the main sources. Poor sanitation and inadequate hygiene practices are major risk factors.[1] Diagnostic approaches include enterotests, antibody detection, and

polymerase chain reaction (PCR), although traditional microscopy of concentrated fecal samples remains a cost-effective and reliable method.[4] While giardiasis often resolves without medical intervention, untreated cases can lead to prolonged symptoms and an increased risk of transmission.[5] Current treatments against giardiasis such as metronidazole (MTZ) and albendazole (ABZ), are facing reduced efficacy due to rising antibiotic resistance, posing a significant challenge.[6,7]

1.1.2. Giardia's adaptation in the mammalian small intestine

Infection begins when a host ingests Giardia cysts, which undergo excystation in the acidic environment of the stomach and proximal small intestine, releasing four trophozoites through cell division.[8] These trophozoites adhere to the intestinal epithelium with their ventral discs, initiating giardiasis symptoms. As they traverse the small intestine, Giardia senses and responds to environmental changes, particularly variations in pH and bile concentrations. Prolonged exposure to a less acidic pH and higher bile levels in the intestinal lumen triggers encystation and subsequent excretion.[9]

The proximal small intestine, with its higher oxygen levels (32 mmHg) compared to the large intestine (3-11 mmHg) and fluctuating oxygen concentrations post-meal,[10] presents a challenging environment for Giardia. Despite this, Giardia thrives in the nutrient-rich proximal small intestine.

As an amitochondriate parasite, Giardia relies on amino acids such as aspartate, alanine, and arginine for energy metabolism.[11] Since it cannot synthesize most amino acids except valine and alanine, the parasite must scavenge them from the intestinal environment.[12] Amino acids are primarily absorbed in the proximal small intestine, which aligns with Giardia's localization to this region. Moreover, Giardia lacks the enzymes

needed to synthesize complex biomolecules like carbohydrates and sterols, depending instead on vacuolar uptake of these nutrients from the host.[13]

The large intestine, which hosts majority of the gut microbiota, acts as a protective barrier, preventing Giardia attachment to the epithelial walls. If trophozoites reach the large intestine, commensal microbes hinder their attachment and compete for nutrients.[14] Overall, Giardia prefers the proximal small intestine due to nutrient availability, favourable pH and bile conditions, and reduced competition from the microbiota.

1.1.3. Giardia taxonomy

While this thesis focuses on *G. intestinalis* (referred to as "Giardia" for simplicity), it is important to recognize that different Giardia species infect different hosts (Table 1). The six most accepted species include *G. intestinalis*, *G. agilis*, *G. ardeae*, *G. microti*, *G. muris*, and *G. psittaci*. Recently, *G. varani* has also been considered a distinct species.[15]

1.1.3.1. Species of Giardia

Giardia species exhibit subtle morphological differences that are challenging to distinguish under a microscope. *G. intestinalis* (syn. *G. lamblia*, *G. duodenalis*) has a characteristic pear-shaped trophozoite with two nuclei, four pairs of flagella, and a prominent ventral adhesive disc.[16] Other species, such as *G. muris* and *G. agilis*, differ primarily in shape and size; *G. muris* is shorter and rounder than *G. intestinalis*, while *G. agilis* is more elongated.[17,18] Despite these differences, they are often too subtle for reliable identification, making molecular techniques like PCR and sequencing essential for accurate species differentiation.[15]

Table 1: Primary hosts of Giardia species.[15]

Giardia species	Major host	Discovered by
G. agilis	Amphibians	Kunstler, 1882
G. ardeae	Birds	Noller, 1920
G. intestinalis	Mammals	Davaine, 1875
G. microti	Muskrats, voles	Benson, 1908
G. muris	Rodents	Benson, 1908
G. psittaci	Birds	Erlandsens & Bemrick, 1987
G. varani	Lizards	Lavier, 1923

1.1.3.2. Subspecies of *Giardia intestinalis*

Once thought to be a single species that infects mammals, *G. intestinalis* is now recognized as a complex of multiple subspecies or assemblages (Table 2). Phylogenetic analyses using small-subunit rRNA and several housekeeping genes, including glutamate dehydrogenase (*gdh*), β-giardin (*bg*), and triosephosphate isomerase (*tpi*), have revealed genetic distinctions among these assemblages.[15]

Giardia assemblages exhibit distinct host specificities. Among the eight recognized assemblages, A and B show the most diversity, infecting humans, pets, and livestock. Assemblage A is further subdivided into AI, AII, and AIII, with distinctions primarily related to host species rather than molecular differences.[19] Assemblages C and D are found in domestic and wild canines, while assemblage E infects livestock and humans. Assemblages F, G, and H infect cats, rodents, and seals, respectively.[15] Assemblages A, B, and E, which can all infect humans are the focus of this thesis, primarily because these are the assemblages that contain my protein of interest.

Table 2: *Giardia intestinalis* assemblages and their commonly infected hosts (not an exhaustive list).[15] * Indicates assemblages examined in this thesis.

***G. intestinalis* assemblage**	**Mammalian hosts**
Assemblage A*	Humans, non-human primates, livestock, pigs, horses, canines, cats, ferrets, marsupials
Assemblage B*	Humans, non-human primates, cattle, dogs, horses, rabbits, beavers, muskrats
Assemblage C	Domestic and wild canines
Assemblage D	Domestic and wild canines
Assemblage E*	Livestock, pigs, humans
Assemblage F	Cats
Assemblage G	Mice, rats
Assemblage H	Seals

1.2. Oxidative stress and Giardia

Oxidative stress arises when reactive oxygen species (ROS) exceed the capacity of antioxidant defenses, leading to significant damage to biomolecules, including carbohydrates, lipids, proteins, and nucleic acids. This damage is implicated in various diseases, including neurodegenerative disorders, cardiovascular diseases, and various inflammatory conditions.[20]

To counteract ROS-induced damage, organisms rely on an array of antioxidant enzymes such as superoxide dismutase (SOD), catalase, and glutathione peroxidase, which collectively work to maintain redox homeostasis. Giardia lacks these common antioxidant defenses but has developed alternative mechanisms to manage oxidative stress, including superoxide reductase (SOR),[21] peroxiredoxins,[22] and NAD(P)H oxidase,[23] which help the parasite cope with fluctuating oxygen levels in the small intestine.

1.2.1. Reactive oxygen species (ROS) and their impact

Reactive oxygen species are highly reactive molecules produced as natural byproducts of oxidative metabolism (Equation 1). While ROS are crucial for cell signaling and apoptosis, they are also implicated in diseases such as cancer and chronic inflammation.[20] Among ROS, superoxide anions ($O_2^{\bullet-}$), hydrogen peroxide (H_2O_2), and hydroxyl radicals ($^{\bullet}OH$) are particularly damaging to biomolecules, including DNA, RNA, membrane lipids, and proteins. For example, hydroxyl radical can induce significant DNA damage leading to mutagenesis and genomic instability which are critical for disease development.[24]

$$O_2 \xrightarrow{e^-} O_2^{\cdot-} \xrightarrow{e^-,\ 2H^+} H_2O_2 \xrightarrow{e^-,\ H^+} \cdot OH \xrightarrow{e^-,\ H^+} H_2O \quad (1)$$

1.2.2. Antioxidant mechanisms in Giardia

Giardia employs various strategies to manage reactive oxygen species (Table 3). SOD typically detoxifies superoxide by converting it to hydrogen peroxide and oxygen. However, Giardia uses SOR to directly reduce superoxide to hydrogen peroxide.[21] While SOR can only consume one molecule of superoxide for every two that SOD can, SOR simultaneously consumes NAD(P)H. This diminishes the overall negative redox status and ultimately, reduces superoxide production. The turnover numbers for SOD and SOR are 10^6 sec^{-1} and 10^{-4} sec^{-1}, respectively, indicating that SOD is much more efficient.

Giardia also lacks catalase and glutathione peroxidase but contains peroxiredoxins, which reduce hydrogen peroxide directly to water.[22] Peroxiredoxins, like peroxidases, can break down various peroxides and not solely hydrogen peroxide as catalase does. These direct strategies effectively prevent the production of oxygen, which is advantageous for a

microaerotolerant organism. Additionally, Giardia contains flavodiiron proteins and NAD(P)H oxidase which detoxify oxygen by converting it to water. These enzymes help Giardia cope with fluctuating oxygen levels in the small intestine, but despite their essential roles, the exact functions of these enzymes remain partially understood.[23]

Table 3: Antioxidant defenses in Giardia and the reactions they catalyze.

Antioxidant defense enzymes	Reaction catalyzed	Found in Giardia?
Oxygen detoxification		
Flavodiiron protein (FDP)	$O_2 \rightarrow H_2O$	Yes[25]
NAD(P)H oxidase	$O_2 \rightarrow H_2O$	Yes[23,26]
Superoxide detoxification		
Superoxide dismutase (SOD)	$2O_2^{\cdot -} + 2H^+ \rightarrow H_2O_2 + O_2$	No[26]
Superoxide reductase (SOR)	$O_2^{\cdot -} + 2H^+ + e^- \rightarrow H_2O_2$	Yes[21]
Peroxide detoxification		
Catalase	$2H_2O_2 \rightarrow 2H_2O + O_2$	No[26]
Glutathione peroxidase	$2GSH + H_2O_2 \rightarrow GSSG + 2H_2O$	No[26]
Peroxiredoxins	$H_2O_2 \rightarrow H_2O$	Yes[22]

1.3. Flavohemoglobins

1.3.1. Nitric oxide and nitrosative stress

Similar to oxidative stress, nitrosative stress arises from an imbalance between reactive nitrogen species (RNS) and cellular defense mechanisms. Nitrosative stress is associated with cell death, mitochondrial dysfunction, and the onset of cardiovascular disease.[27] Nitric oxide ($^{\bullet}NO$), a prominent RNS, plays a vital role in maintaining intestinal mucosal membranes and regulating various physiological functions.[28]

Nitric oxide synthases (NOS) are a class of heme-containing enzymes that catalyze the two-step oxidation of arginine to citrulline using oxygen and NADPH. Mammals contain three NOS variants: neuronal, endothelial, and inducible NOS, which contribute to neurotransmission, vasoregulation, and host defense.[29] Since Giardia exclusively replicates in the lumen of the small intestine, nitric oxide production by intestinal epithelial cells would be expected to play a major role in clearing the infection. However, neuronal NOS is the most critical, as it regulates gut motility. Without neuronal NOS activity, Giardia infections persist.[29]

To counteract nitric oxide production, Giardia uses arginine deiminase to limit arginine availability, the substrate for nitric oxide synthesis.[30] However, Giardia's primary direct strategy for nitric oxide detoxification is flavohemoglobins, which provide a more direct and efficient approach for nitric oxide detoxification.

1.3.2. Flavohemoglobin, a key enzyme in nitric oxide detoxification

Flavohemoglobins catalyze the conversion of nitric oxide to nitrate (NO_3^-), alleviating nitrosative stress (Figure 1). The enzyme's catalytic cycle involves molecular oxygen binding to the ferrous (Fe^{2+}) heme group, forming a superoxide-ferric (Fe^{3+}) complex that reacts with nitric oxide.[31] The ferric heme is then restored to the ferrous state through the acceptance of an electron from the flavin cofactor FAD. Flavohemoglobins use the nicotinamide cofactors NADH and NADPH as electron donors, though flavohemoglobins have a higher affinity towards NADH.[32] While these cofactors provide electrons in pairs, the reaction cycle requires only a single electron; hence, FAD acts as an intermediary, accepting pairs of electrons from NAD(P)H and donating them singly to heme.

In addition to their nitric oxide dioxygenase activity, flavohemoglobins exhibit NADH oxidase activity, transferring electrons from NADH through FAD, FMN, and finally to the heme group and oxygen. This activity persists even in the absence of nitric oxide, albeit at reduced rates, suggesting that NADH may have other molecular targets or pathways, which warrants further investigation.[33]

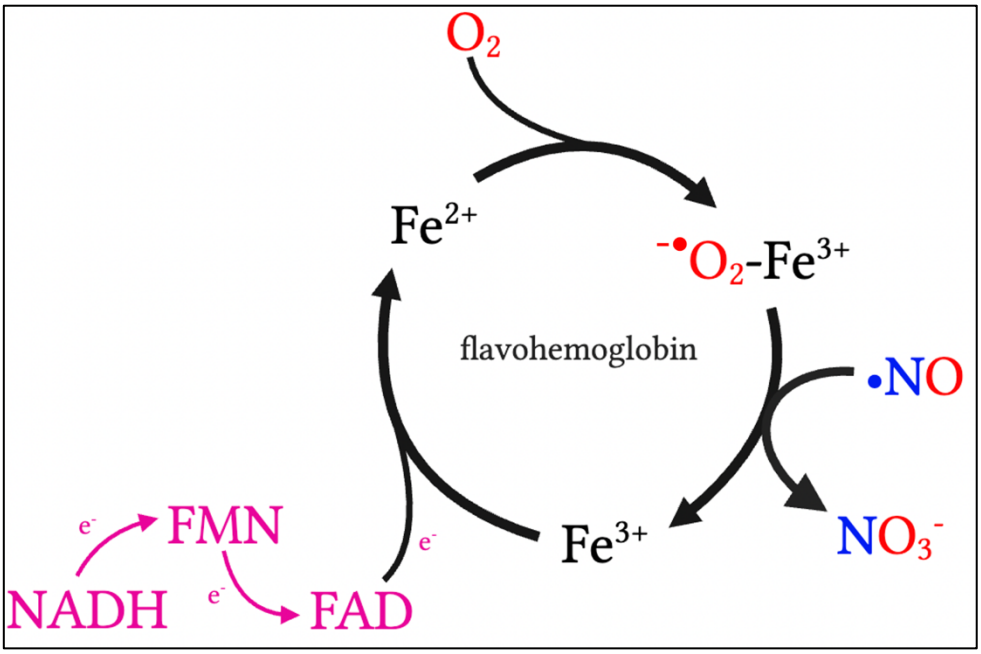

Figure 1: The catalytic cycle of flavohemoglobins. The cycle is divided into two key activities: NADH oxidase activity (pink) and nitric oxide dioxygenase activity (black). NADH donates two electrons to the flavin cofactors, which then transfer them to heme (Fe^{3+}) to convert nitric oxide ($^{\bullet}NO$) to nitrate (NO_3^-). Image created using BioRender.

1.3.3. Structural characteristics of flavohemoglobins

Flavohemoglobins possess a dual-domain structure consisting of an amino-terminal globin domain and a carboxy-terminal ferredoxin $NADP^+$ reductase (FNR) domain (Figure 2). The globin domain, responsible for heme binding, features a helical fold that stabilizes the heme and positions the iron for effective ligand interaction. The heme-binding pocket is surrounded by six α-helices (helices B-G), a structural arrangement that

creates a hydrophobic environment conducive to heme stabilization and that is highly conserved among other globins, such as hemoglobin and myoglobin.[34]

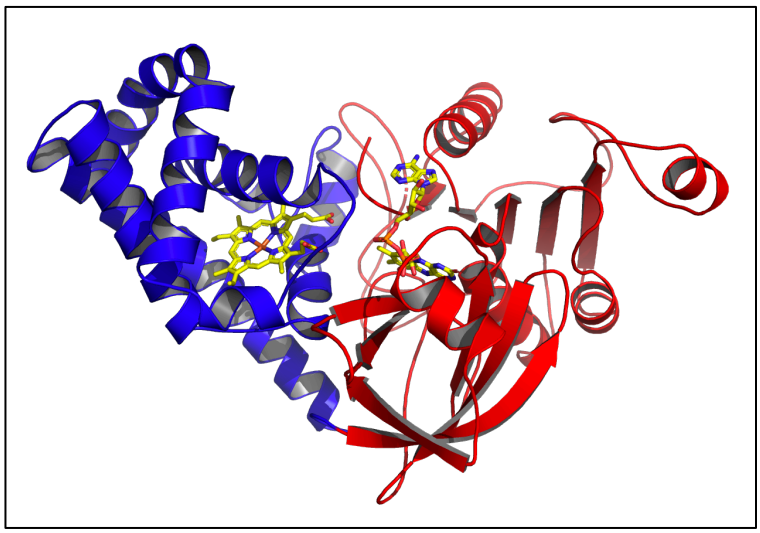

Figure 2: Structure of *E. coli* flavohemoglobin (Hmp) where the amino-terminal globin domain is depicted in blue, and the carboxyl-terminal FNR domain is depicted in red. Heme and FAD groups are pictured in yellow. Image was generating using PyMOL.

Unlike mammalian globins, flavohemoglobins lack a distal histidine, which typically aids in oxygen binding.[35] Instead, flavohemoglobins rely on alternative residues, such as leucine (L58, helix E), tyrosine (Y30, helix B), and glutamine (Q54, helix E) to stabilize bound oxygen and facilitate its activation for further reactions rather than reversible binding (Figure 3). Despite the absence of the distal histidine, the proximal histidine (H107, helix F) remains crucial for coordinating the heme iron and binding oxygen.[35] This proximal histidine forms a hydrogen bond with an adjacent glutamic acid residue (E157, helix H), increasing its electronegativity and enhancing its role in oxygen activation. This interaction stabilizes the histidine in an imidazolate-like state, a characteristic often observed in peroxidases, where it facilitates efficient electron transfer during peroxide reduction.[36] Moreover, structural shifts in flavohemoglobins create additional ligand-binding sites essential for their unique enzymatic functions.[28]

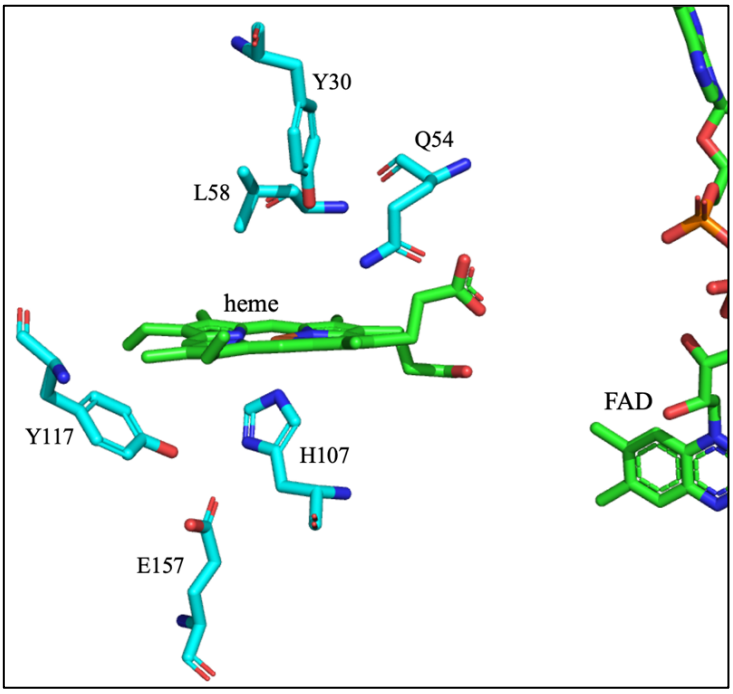

Figure 3: Conserved amino acid residues in the heme-binding site of flavohemoglobins. Heme is pictured in green and the residues in cyan. Oxygen is labelled in red and nitrogen in blue. Image generated using PyMOL.

The FNR domain consists of two regions: a six-stranded antiparallel β-barrel structure (FAD-binding domain) and a five-stranded parallel β-sheet (NADH-binding domain).[37] Interactions between NADH, FAD, and the heme group are vital for electron transfer. Interestingly, truncated hemoglobins, which lack the FNR domain of flavohemoglobins, also exhibit nitric oxide dioxygenase activity, converting nitric oxide to nitrate.[38] This suggests that the FNR domain may not be strictly required for this function, but its presence likely enhances the overall catalytic efficiency.

Flavohemoglobins exhibit significant conformational changes during their catalytic cycle, which are essential for their function. These changes include adjustments in the heme pocket to accommodate ligand binding, flexibility between the globin and FNR domains to optimize electron transfer, and alterations in the orientation of FAD and FMN

to enable effective nitric oxide oxidation. These dynamic features highlight the enzyme's ability to transition between various functional states, enhancing its role in managing reactive nitrogen species.[39,40]

1.3.4. Inhibition of flavohemoglobins

Flavohemoglobin inhibition has been extensively studied in *Escherichia coli* flavohemoglobin, known as Hmp, with inhibitors that target the heme group emerging as possible candidates for giardiasis treatment. Inhibition of the nitric oxide dioxygenase activity of flavohemoglobins could disrupt a key protective mechanism, potentially harming its host organism.[41] Imidazole-based drugs, particularly those with bulky aromatic substituents, may offer selective inhibition of the nitric oxide dioxygenase activity, as they coordinate the heme group and fit inside the large distal hydrophobic pocket. Exploration of the effect of inhibitors of the NADH oxidase activity could provide insight into the functional significance of this activity, reveal conditions that promote reactive oxygen species formation, and establish flavohemoglobins as potential drug targets.[42]

1.3.5. Flavohemoglobins and lipids

While flavohemoglobins are primarily known for their nitric oxide dioxygenase activity, evidence suggests they may also interact with lipids and have a role in lipid metabolism. Structural studies on Hmp and *Alcaligenes eutrophus* flavohemoglobin (FHP) reveal that these proteins coordinate heme and bind fatty acids.[37] Hmp selectively interacts with unsaturated and cyclopropanated fatty acids, transitioning the heme iron from a penta-coordinated to hexa-coordinated high spin state.[43] Flavohemoglobins

selectively recognize cis-double bonds while excluding saturated fatty acids and hydrocarbons, including those found in phospholipids. Lipids, which are thought to occupy a cavity on the distal, oxygen-binding face of the heme group, influence the heme coordination and ligand interactions with imidazole, oxygen, and carbon monoxide.[43]

In FHP, X-ray crystallography has identified a hydrophobic phospholipid-binding site adjacent to the heme group, suggesting that lipid interactions may be a conserved feature among flavohemoglobins.[37] While flavohemoglobins are generally cytosolic, these phospholipid interactions raise the possibility that they may transiently associate with membranes under certain conditions, potentially regulating activity or responding to cellular stress.[37] Membrane localization could position flavohemoglobins near the site of lipid peroxidation, allowing them to mitigate oxidative damage.

In Giardia, which relies on lipid scavenging rather than *de novo* synthesis, the composition of available lipids may directly influence flavohemoglobin function.[12] Investigating these interactions could provide insight into how flavohemoglobins contribute to lipid homeostasis and metabolism in Giardia.

1.3.6. Giardia flavohemoglobin (gFlHb)

Among flavohemoglobins, Giardia flavohemoglobin (gFlHb) particularly stands out. Flavohemoglobins are among the most abundant globin genes,[44] with a total of 6249 sequences identified, including 6111 from bacteria and 116 from eukaryotes. Most bacterial flavohemoglobins are found within the Proteobacteria phylum, with Hmp being the most extensively studied.[45]

Giardia intestinalis possesses a flavohemoglobin[33] not found in other Giardia species,[46] which is important for its survival in the oxygen-variable environment of the

mammalian gastrointestinal tract.[47,48] Interestingly, as an amitochondriate, Giardia cannot synthesize heme, yet it still encodes five heme proteins, one of which is gFlHb. This makes gFlHb particularly intriguing, as its inability to produce heme forces the uptake of this cofactor from external sources. In addition, flavohemoglobins have only been identified in Giardia assemblages A, B, and E, an intriguing discovery which may be a result of chance, or rather a specific adaptation important for survival of the human gut. While full genome analyses have yet to be performed on assemblages F, G, and H, no flavohemoglobin was identified in assemblages C and D, which predominantly infect canines.[19]

Unlike the well-characterized bacterial flavohemoglobins, gFlHb exhibits distinct structural and functional features (Figure 4). Like other flavohemoglobins, gFlHb possesses nitric oxide dioxygenase activity and its expression is upregulated in response to nitrosative stress.[33] Comparative analysis reveals that gFlHb has a higher sequence identity with Hmp (42%) than with other eukaryotes like *Saccharomyces cerevisiae* (33%), suggesting that Giardia acquired its flavohemoglobin through horizontal gene transfer from a Gram-negative bacterial source.[49] Notably, gFlHb is larger (52 kDa) than all other reported flavohemoglobins, which typically weigh around 44 kDa (Figure 5). This increased size is primarily due to two amino acid sequence inserts: one in the globin domain (residues 74-94) and another in the FNR domain (residues 281-310). Molecular modeling with AlphaFold suggests that these inserts interact with each other, enhancing the contact surface between the domains and facilitating intradomain interactions. Despite these insights, much remains unknown about gFlHb, highlighting a significant gap in our understanding.

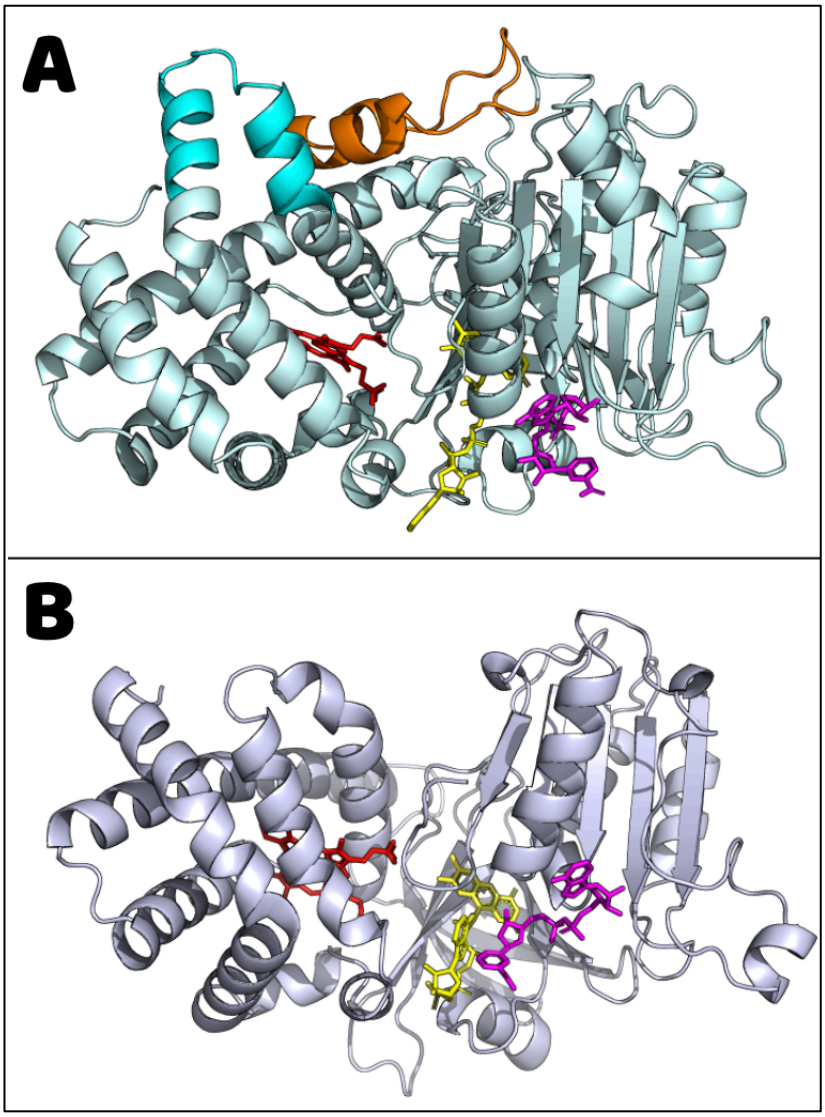

Figure 4: **(A)** Structure of Giardia flavohemoglobin (gFlHb), where sequence inserts are highlighted in cyan (globin domain) and orange (FNR domain). **(B)** *E. coli* flavohemoglobin (Hmp, 1GVH.pdb). In both panels, the heme group is shown in red, the FAD cofactor in yellow, and NADH in magenta. Images were generated using AlphaFold3 and PyMOL.

Figure 5: Sequence alignment of gFlHb and Hmp. The inserts are highlighted in cyan (globin domain) and orange (FNR domain). Asterisks indicate identical residues, while colons and periods indicated similar residues.

1.3.6.1. gFlHb in oxidative stress response

Flavohemoglobins have been extensively studied for their role in nitrosative stress, primarily due to their high nitric oxide dioxygenase turnover rates and gene upregulation in response to nitric oxide.[47] However, recent evidence suggests they may also play a crucial role in oxidative stress management. A transcriptomic analysis of Giardia trophozoites exposed to oxygen and hydrogen peroxide revealed a substantial upregulation of gFlHb under these conditions.[50] Given that Giardia lacks SOD and catalase, gFlHb may function as a compensatory antioxidant mechanism, working alongside other enzymes like SOR and peroxiredoxins.

Interestingly, Hmp exhibits hydrogen peroxide reductase activity, although it is more efficient at reducing alkyl peroxides.[51] Under anaerobic conditions in the presence of NADH, Hmp can reduce peroxide to alcohol and water. Furthermore, kinetic studies have demonstrated that the ferric reductase activity of flavohemoglobins is sensitive to inhibition by SOD under aerobic conditions, consistent with superoxide formation by the enzyme.[52] Additionally, Hmp expression increases under oxidative stress, leading to increased superoxide production. While Hmp knockouts strains display a decreased ability to combat oxidative stress, the overall survival of *E. coli* remains unaffected.[53]

X-ray crystallography[40] and Raman resonance spectroscopy[54] reveal structural similarities between the heme-binding pocket of Hmp and gFlHb and the active sites of classical type I and II peroxidases. This suggests a potential role for gFlHb in peroxide metabolism and reinforces the idea that Giardia has evolved alternative mechanisms to manage oxidative stress in the absence of conventional antioxidant enzymes.

1.4. Thesis aims

1. **Characterize flavohemoglobin variants:**
    - **Compare the NADH oxidase activity of Hmp and gFlHb from assemblages A, B, and E.** These are the only Giardia assemblages known to infect humans and have identified flavohemoglobins. Understanding their responses to various conditions including oxidative stress and inhibition may provide insights into biochemical adaptations, evolutionary differences, and potential variations in pathogenicity and virulence.

2. **Study lipid-flavohemoglobin interactions:**
    - **Confirm lipid binding to gFlHb and identify variations in lipid content among assemblages.** Since lipids are known to bind Hmp, it is important to verify whether this interaction is conserved across flavohemoglobin variants and whether different flavohemoglobins bind distinct lipids.
3. **Elucidate the role of gFlHb in oxidative stress response:**
    - **Study the effect of hydrogen peroxide on the NADH oxidase activity of gFlHb, and conditions of hydrogen peroxide generation or consumption.** Flavohemoglobins are most often implicated in nitrosative stress, however a role in oxidative stress would expand our knowledge on the functional capabilities of gFlHb.

2. MATERIALS AND METHODS

2.1. Protein expression

2.1.1. Transformation

Expression vectors (Bio Basic, Markham ON) for Hmp and gFlHb were based on the pET-14b backbone, conferring ampicillin resistance and encoding recombinant proteins with N-terminal hexa-histidine tags. These tags are advantageous for purifying recombinant proteins via nickel affinity chromatography.

To express flavohemoglobins, the vectors encoding the protein were first transformed into *E. coli* BL21(DE3) cells, a protease-deficient cell line that encodes T7 RNA polymerase on the DE3 lysogen, ideal for high-yield protein production. The transformation procedure followed the protocol outlined by New England Biolabs.[55] Specifically, 50 µL of competent BL21(DE3) cells were thawed on ice for ten minutes, and 2 ng of the expression vector was added. After incubation on ice for 30 minutes, the cells were heat-shocked at 42°C for ten seconds and returned to ice for five minutes. Next, 950 µL of SOC medium was added, and the cells were grown at 37°C for one hour. Selective LB-agar plates containing 100 µg/mL ampicillin were warmed, inoculated with 20 µL of the transformed cells, and incubated at 37°C overnight. The following day, a single colony was picked and grown in 2 mL LB medium containing 100 µg/mL ampicillin overnight at 37°C (250 rpm). The culture was supplemented with 2 mL of 50% sterile glycerol, and 100 µL aliquots were stored at -80°C.

2.1.2. Autoinduction of recombinant flavohemoglobin variants

For protein expression, one aliquot of the transformed cells was inoculated into 2 mL LB broth containing 100 µg/mL ampicillin and grown overnight (12-18 hours) at 37°C (250 rpm). A 0.5 mL portion of this starter culture was then transferred into a sterile 250 mL flask containing 50 mL LB broth supplemented with 30 µg/mL ampicillin, 0.2% lactose, 0.5% glycerol, 0.05% glucose, 2 mM $MgSO_4$, 0.1 mM ALA (to stimulate heme synthesis), 0.05 mM $FeCl_3$, 0.02 mM $CaCl_2$, and 5X trace metals (0.01 mM $MnCl_2 \bullet 4H_2O$, 0.01 mM $ZnSO_4 \bullet 7H_2O$, 0.002 mM $CoSO_4 \bullet H_2O$, 0.002 mM $CuSO_4 \bullet 5H_2O$, 0.002 mM $NiSO_4 \bullet 6H_2O$, 0.002 mM H_3BO_3). These conditions were optimized to maximize protein expression. The culture was incubated for 18-24 hours at 37°C (250 rpm), and the cells were harvested by centrifugation at 9000 *g* for 10 minutes at 4°C. The cell pellets were stored at -80°C. In the case where purification was done on the same day as harvesting, purification was found to be more effective after a freeze-thaw cycle.

2.2. Protein purification

To begin purification, cell pellets were thawed refrozen three times in liquid nitrogen before being resuspended in 5 mL of loading buffer (20 mM K_3PO_4, 300 mM KCl, and 10 mM imidazole, pH 7.4) per gram of pellet. The cells were lysed by sonication (80% intensity, 20 seconds per pulse, total of 2 minutes) using a Fisher Scientific Model 100 Sonic Dismembrator. The lysate was then centrifuged at 9000 *g* for 20 minutes at 4°C. The supernatant, containing flavohemoglobin, was applied to a 1 mL Ni-NTA affinity column (Qiagen #30210). The column was washed with 10 mL loading buffer, followed by 8 mL wash buffer (20 mM K_3PO_4, 300 mM KCl, 25 mM imidazole, pH 7.4) to remove

impurities. The protein was then eluted with elution buffer (20 mM K_3PO_4, 300 mM KCl, 400 mM imidazole, pH 7.4). The semi-purified protein was concentrated using Amicon Ultra-15 filtration units (30 kDa), centrifuged at 4000 g for 10 minutes at 4°C, and further purified using an FPLC equipped with 24 mL Superdex-200 Increase 10/300 GL gel filtration column and equilibrated with 100 mM K_3PO_4 (pH 7.4) at a flow rate of 0.75 mL/min. The reddest fractions were pooled and stored in 50% glycerol at -20°C.

Protein concentration was determined via spectrophotometric measurements of the Soret band, a peak between 400 and 410 nm that corresponds to the maximum heme absorbance of flavohemoglobins. The UV-visible spectra of the purified flavohemoglobin were recorded at room temperature from 250-700 nm using a Shimadzu UV-visible 1900i spectrophotometer baseline corrected in 100 mM K_3PO_4 (pH 7.4). The experimentally determined extinction coefficient (139.7 $mM^{-1}cm^{-1}$) was used to calculate the protein concentration (Beer-Lambert's law; $Absorbance = \varepsilon C l$, where ε is the extinction coefficient, C is the concentration, and l is the path length of the cuvette).

To verify the purity of flavohemoglobins, 12% SDS-PAGE gels were run using a Bio-Rad mini-gel system. An unstained molecular weight ladder, ranging from 10-250 kDa (Biolabs #P7704S) was loaded into the first lane of each gel. The electrophoresis was conducted at 120 V through the stacking gel, followed by 150 V through the separating gel in 1X Tris-glycine SDS running buffer, continuing until the dye front ran off the gel. Subsequently, gels were stained with Coomassie Brilliant Blue and destained in water overnight on an orbital shaker. The following day, the gels were imaged and analyzed using Image Lab 6.0.1 software.

2.3. UV-Visible spectrophotometric kinetics

2.3.1. NADH oxidase activity

Rate measurements were conducted using a Shimadzu UV-1900i UV-Visible spectrophotometer connected to an RX2000 rapid flow kinetic accessory equipped using the narrow optical window with a 1 cm path length (Figure 6). This accessory facilitates stopped-flow rate measurements by loading reagents into drive syringes, which are then delivered through a mixing chamber into a specialized microcuvette for 60-second kinetic runs. Each kinetic run has a reaction volume of 200 μL, with the results from a minimum of fifteen runs typically averaged for each condition. The measurements were carried out in 100 mM Bis-Tris buffer (pH 6.5) containing 200 μM NADH in one syringe, and 0.05-1 μM flavohemoglobin and 2 μM FAD in the other. Reagent concentrations are halved upon mixing. In certain experiments, 1 mM hydrogen peroxide, 1 mM imidazole, 1 mM sodium cyanide, 1 mM sodium nitrite, and 20 μM miconazole were mixed in both syringes. Temperature was maintained at 37°C using a circulating water bath connected to the flow accessory. The oxidation of NADH was monitored by measuring the decrease in absorbance at 340 nm from which specific activities, corresponding to the number of moles of NADH oxidized per minute per mole of enzyme, were calculated (using an $\varepsilon_{340} = 6.22\ mM^{-1}cm^{-1}$ for NADH).

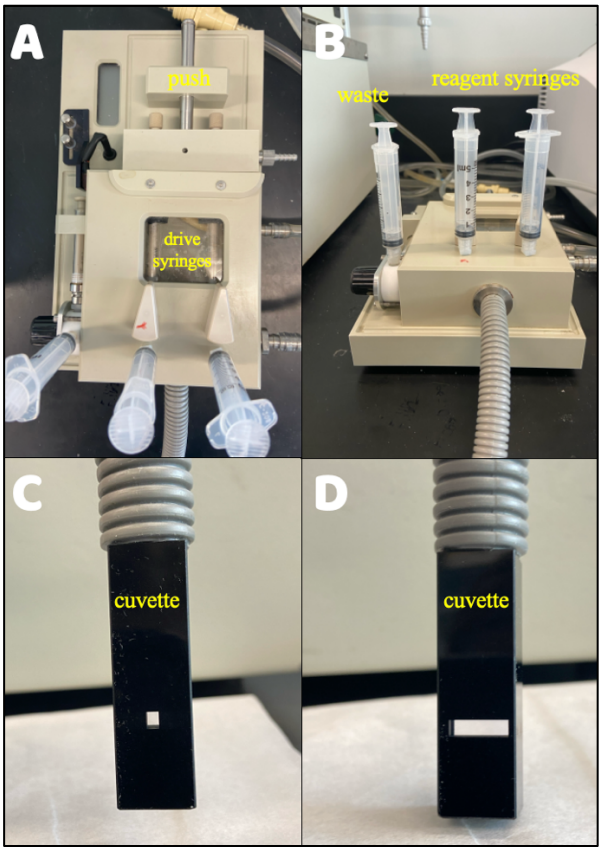

Figure 6: RX2000 flow accessory for kinetic experiments connected to an external water bath set to 37°C. **(A)** Configuration of the flow accessory, highlighting the two reagent syringes and the waste syringe (positioned leftmost). One reagent syringe is preloaded with 0.05-1 µM enzyme and 2 µM FAD in 100 mM Bis-Tris buffer (pH 6.5), while the second syringe contains 200 µM NADH in the same buffer. **(B)** Solutions are drawn into the drive syringes and 100 µL of each solution is delivered through a mixing chamber into the specialized microcuvette. The cuvette is placed in the UV-visible spectrophotometer with the optical window oriented towards the light path, using either the 0.2 cm **(C)** or the 1 cm **(D)** path length.

2.3.2. Cytochrome *c* reductase activity

Reduction assays were performed in a quartz cuvette, with a 1 cm path length and total volume of 3 mL. 25 µM ferricytochrome *c*, 1 µM FAD, and 0.05-0.2 µM flavohemoglobin were mixed in the cuvette with 100 mM Bis-Tris buffer (pH 6.5). Reactions were initiated by the addition of 100 µM NADH and measurements followed the increase in ferricytochrome *c* reduction by the absorbance increase at 550 nm as ferrocytochrome *c* was formed. An orange to pink colour change is observed. Rates were

again reported in terms of specific activity (using an ε_{550} = 22.1 $mM^{-1}cm^{-1}$ for the absorbance difference between ferro and ferricytochrome *c*). In certain cases, 5 U/mL SOD (Worthington Biochemicals) was included in assays to determine the contribution of superoxide to the rate of cytochrome *c* reduction.

2.4. gFlHb variants and mutants

Mutations were selected based on their predicted effect on the stability of gFlHb. Careful analysis of the residues within the sequence inserts on PyMOL revealed a close-contact interaction between a tryptophan (W90) and methionine (M299) residue, each located in one of the two inserts of the protein (Figure 7). To disrupt this interaction, both residues were mutated to alanine, a common strategy to eliminate aromatic-sulfur interactions, which are important in protein folding. The mutant pET14b vector "gFlHb W90A/M299A" was ordered from Bio Basic (Markham, ON). Mutant vectors, as well as gFlHb B and E were transformed, expressed, and purified in the same manner as the wild type flavohemoglobins and were assayed in an identical manner.

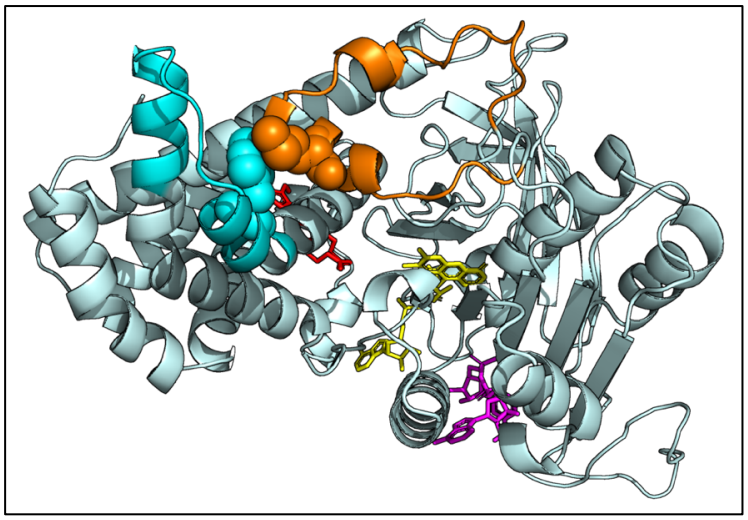

Figure 7: Ribbon presentation of gFlHb illustrating the side chains of W90 (cyan) in the N-terminal insert and M299 (orange) in the C-terminal insert depicted as spheres to highlight their interactions. Image generated using PyMOL.

2.5. Optical binding studies

Binding studies of ferric and ferrous gFlHb were performed in 100 mM Bis-Tris buffer (pH 6.5) in a 3.5 mL quartz cuvette using a Shimadzu UV-1900i UV-visible spectrophotometer. Spectra were recorded from 250-700 nm, with particular attention to the Soret peak (400-410 nm) and the Q bands (500-600 nm). Protein solutions (1-2 μM gFlHb) were treated with 100 μM NADH to generate the oxygenated heme state and with 10 mM sodium dithionite to produce the deoxygenated heme state. Ligand binding was assessed by adding 1 mM imidazole, 20 μM miconazole, 1 mM sodium nitrite, 1 mM sodium cyanide, to the ferric, oxygenated, or deoxygenated forms of gFlHb in separate experiments. In order to avoid introducing oxygen, especially into the dithionite-treated protein sample, inhibitors were added prior to the reducing agents.

2.6. Lipid extraction and removal

Lipids were extracted from the protein sample by mixing 333 μL of concentrated protein with 333 μL chloroform and 667 μL methanol. The mixture was vortexed for 30 seconds. An additional 333 μL chloroform and 333 μL deionized water were added, and the mixture was vortexed again for 30 seconds. Samples were microcentrifuged for 2 minutes at 12000 rpm, after which the top aqueous layer and any pelleted protein were removed, leaving lipids in the chloroform layer. The chloroform layer was spotted onto silica G thin-layer chromatography (TLC) plates (Macherey-Nagel #805023) and run in a 3:2 hexanes: ethyl acetate solvent system. Lipids were visualized by exposure to iodine vapour for 5 minutes, followed by imaging under UV light.

To determine the lipid compositions of different protein samples, lipid extracts were analyzed using a Thermo QExactive Orbitrap electrospray ionization (ESI) mass spectrometer. Samples were run in both positive and negative ionization modes, with clearer peaks observed in negative mode.

To remove lipids from native protein samples, proteins were applied to one of three column types: ceramic hydroxyapatite (CHT) (BioRad #1584000), Sephadex LH-20 (Cytiva #17009010), or hydroxylalkoxypropyl-dextran (Sigma #H6383). These columns are collectively referred to as lipidex columns for simplicity. The CHT column is a calcium phosphate resin which binds proteins through interactions between the resin's negatively charges phosphate groups and the protein's positively charged amino groups. Any loosely bound lipids were washed off with 5 mM potassium phosphate buffer (pH 7), and proteins were subsequently eluted with a 10-50 mM potassium phosphate buffer gradient (pH 7), typically eluting between 15-30 mM. In contrast, the Sephadex LH-20 and hydroxylalkoxypropyl-dextran columns selectively retain lipids while allowing proteins to pass through. Proteins were washed and eluted using 25 mM potassium phosphate buffer (pH 7).

2.7. Hydrogen peroxide generation

A horseradish peroxidase (HRP) and o-dianisidine (ODA) assay was used to indirectly measure hydrogen peroxide formation by gFlHb. NADH oxidase activity reactions (100 mM NADH, 1 μM FAD, 1 μM gFlHb in 100 mM Bis-Tris buffer, pH 6.5) were run until NADH was completely oxidized, as NADH interferes with the reaction. Then, 1 mL of this solution was added to 1 mL of the HRP/ODA solution (0.05 mg/mL = 0.475 U/mL HRP and 0.1 mg/mL ODA in 100 mM Bis-Tris, pH 6.5). The reaction was

left for 15 minutes, and qualitative observations were made. To confirm hydrogen peroxide generation, 10 U/mL catalase was added to a control reaction.

To obtain more quantitative results, 100 μM NADH was added to initiate a reaction containing 1 μM FAD, 1 μM gFlHb, 0.475 U/mL HRP, and 0.1 mg/mL ODA in 100 mM Bis-Tris (pH 6.5). A simultaneous measure of the A_{340} (NADH oxidation) and A_{460} (ODA oxidation) was recorded for 5 minutes, until well after all NADH was depleted. Repeat additions of 100 μM NADH were made to the same solution and repeat measurements were taken.

For direct measurements of hydrogen peroxide production, reactions were monitored on a World Precision Instrument free radical analyzer equipped with hydrogen peroxide-sensitive (ISO-HPO2) and oxygen-sensitive (ISO-OXY2) electrodes, and a temperature probe connected to an analog digital converter controlled by Labscribe recording software. Assays were conducted on a 2 mL scale in a World Precision Instrument water-jacketed four-port closed chamber (NOCHM-4) with temperature control via an external circulating water bath (Figure 8). The hydrogen peroxide electrode was calibrated prior to use in 100 mM Bis-Tris buffer (pH 6.5) at 37ºC. Aliquots of a 10 mM hydrogen peroxide standard were added to measure the current response and prepare a standard curve. 1 μM FAD, 100 μM NADH, and 0.5 μM gFlHb were mixed in the reaction chamber and hydrogen peroxide generation was measured through changes in current. A calibration curve was generated using a known hydrogen peroxide standard to convert current changes to changes in hydrogen peroxide concentration.

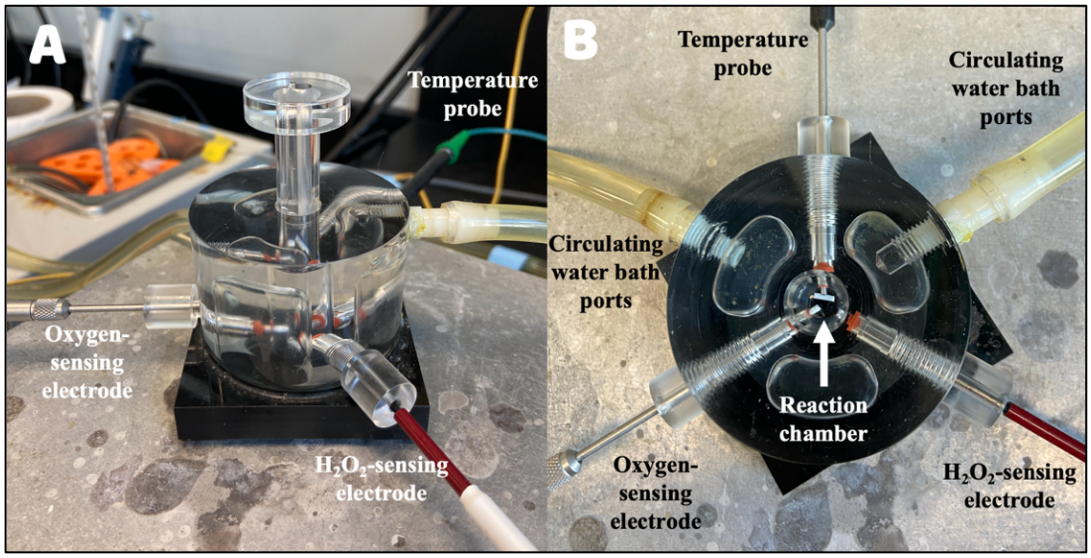

Figure 8: World Precision Instrument free radical analyser side view **(A)** and top view **(B)**. The H_2O_2-sensing and oxygen-sensing electrodes and temperature probe are in a water-jacketed chamber controlled by a circulating water bath set to 37ºC. Assays are conducted in the 2 mL reaction chamber with a stir bar to mix solutions.

2.8. Statistical analyses

All statistical analyses were performed using R (R Core Team 2024) and RStudio (Posit Team 2024). A one-way analysis of variance (ANOVA) was used to test for significant differences in specific activities between gFlHb A, B, and E. If results were significant, a pairwise comparison (Tukey's HSD) was used between groups. Specific activities of gFlHb and Hmp in presence and absence of SOD, and of wildtype gFlHb and gFlHb W90A/M299A mutant were compared using two-sample non-parametric *t*-tests.

3. RESULTS & DISCUSSION

3.1. Catalytic differences between flavohemoglobins of *G. intestinalis* and *E. coli*

The NADH oxidase activity of Hmp (-48.5 min^{-1}, $n = 76$) was nearly threefold higher than that of gFlHb (-17.5 min^{-1}, $n = 111$) (Table 4). Statistical analyses revealed a significant difference in the mean activity between gFlHb and Hmp ($t_{90.4} = 13.927$, $P < 0.0001$). There is a 95% chance that the true specific activity of Hmp is 2.5 to 2.8 times greater than its gFlHb counterpart.

Table 4: NADH oxidase and cytochrome c reductase specific activities of gFlHb, Hmp, and gFlHb W90A/M299A. Where used, 5 U/mL Cu/Zn SOD was added.

Assay	Specific activity (min^{-1})		
	gFlHb	**Hmp**	**gFlHb W90A/M299A**
NADH oxidase	-17.5 ± 7.1	-48.5 ± 18.5	-6.9 ± 2.4
Cyt. *c* reductase	121.9 ± 15.1	90.9 ± 18.9	83.5 ± 21.0
Cyt. *c* reductase + SOD	120.7 ± 11.3	66.6 ± 8.9	83.6 ± 27.6

The primary structural difference between Hmp and gFlHb is the presence of unique sequence inserts in gFlHb. While the exact function of these inserts remains unclear, they are predicted to stabilize the protein by enhancing intradomain interactions between the globin and FNR domains.[33] These inserts may also influence the protein's affinity for oxygen, as reflected in the K_m values of gFlHb (22 ± 7 μM)[56] and Hmp (90 μM),[57] indicating that gFlHb binds oxygen more tightly than Hmp and reaches saturation at lower concentrations. Despite this, NADH oxidase activity is higher in Hmp compared to

gFlHb, suggesting that Hmp compensates for its lower oxygen affinity with a higher turnover number. The looser domain association in Hmp may facilitate a less constrained electron transfer pathway, allowing for a faster reaction cycle once oxygen is bound. In contrast, the sequence inserts in gFlHb could bring the two domains closer together, creating a more restricted electron transfer channel. Furthermore, the flexibility of an enzyme's active site can influence substrate binding and catalysis of different reactions.[58] This structural difference may allow gFlHb to function efficiently under low-oxygen conditions, while Hmp, with its weaker oxygen binding but higher activity, may be optimized for environments where oxygen is more abundant. Giardia's adaptation to a microaerophilic environment suggests that its flavohemoglobin may not prioritize NADH oxidase activity to the same extent as Hmp, supported by the tighter coupling of gFlHb's nitric oxide dioxygenase activity to its NADH oxidase activity relative to Hmp.[59]

In the absence of nitric oxide, the path of electrons from NADH is unknown. In Hmp, elevated NADH oxidase activity can lead to considerable superoxide generation. Purified Hmp was found to reduce exogenous iron (III) citrate in a SOD-sensitive manner, indicating the generation of superoxide during aerobic NADH oxidation.[52] Similarly, to track the path of electrons in gFlHb, cytochrome *c* was added as a terminal electron acceptor. gFlHb exhibited higher cytochrome *c* reductase activity than Hmp, an unexpected finding considering the NADH oxidase activity of Hmp is higher than that of gFlHb (Table 4). This may suggest an alternative electron transfer mechanism, and investigating potential direct protein-protein interactions could help clarify this. The mean specific activities for reduction of cytochrome *c* by Hmp with and without SOD are 66.6 min^{-1} and 90.9 min^{-1} ($t_{22.6} = 3.034$, $P = 0.006$), respectively. For gFlHb, cytochrome *c* reductase activity does not seem to involve superoxide as the specific activity in the

absence of SOD (121.9 min^{-1}) is the same as in its presence (120.7 min^{-1}; $t_{16.7} = 0.203$, $P = 0.8416$). Electron transfer could occur through direct interaction between the proteins, indirectly via superoxide generated by the flavohemoglobin, or a combination of both. Notably, a portion (26%) of Hmp's cytochrome *c* reductase activity was inhibited by SOD, yet there was minimal reduction in gFlHb's activity (< 1% reduction), which supports the hypothesis that electron transfer between flavohemoglobin and cytochrome *c* largely occurs by protein-protein interaction for Hmp and exclusively so for gFlHb. As previously noted, Giardia lacks SOD, which may exert selective pressure on its oxidoreductases to minimize superoxide production as a by-product.

To explore the role of sequence inserts in gFlHb, a mutation targeting W90 in the N-terminal insert and M299 in the C-terminal insert was introduced. Aromatic (from tryptophan) and sulfur (from methionine) interactions are known to stabilize protein structures.[60] By disrupting these potentially important interactions, the two domains of gFlHb may exhibit a looser association, bearing more resemblance to Hmp. However, wildtype gFlHb exhibited a significantly higher NADH oxidase activity (-17.5 min^{-1}) compared to the W90A/M299A mutant (-6.94 min^{-1}; $t_{53.0} = -9.177$, $P < 0.0001$) (Table 4). In addition, despite the reduction in cytochrome *c* reductase activity, no evidence of superoxide formation was found. Activity in the absence of SOD was 83.5 min^{-1}, and this value did not change upon the addition of SOD (83.6 min^{-1}; $t_{39.1} = 0.014$, $P = 0.9887$).

Disrupting the methionine-tryptophan interaction may have caused gFlHb to 'open-up' excessively, weakening the interactions between the globin and FNR domains and leading to less efficient electron transfer from the flavin to heme. Since electron transfer rates decrease exponentially with increasing distance between the electron donor and acceptor,[61] this structural change could significantly impair their function. Alternatively,

the removal of two relatively bulky amino acids could have allowed surrounding residues to come even closer together, creating a tighter association between domains. This could explain the decrease in NADH oxidase activity observed in the double mutant compared to wildtype, like what is seen in Hmp. A tighter domain association may force electrons down a more restricted path, limiting their flow.

Further research is needed to explore these possibilities, starting with the analysis of the single mutants, W90A and M299A, as well as the potential impact of fully deleting the inserts. While there is concern that complete deletion might destabilize the protein, this experiment could offer definitive insight of the inserts' role in maintaining the structural integrity of the protein. Additionally, thermostability studies on both the wildtype and double mutant proteins could clarify whether the disruption of this interaction destabilized the protein as initially expected.

3.2. Structural and kinetic differences in gFlHb from assemblages A, B, and E

Expression levels of gFlHb were comparable across assemblages A, B, and E. As a heme protein, gFlHb's natural red colour allowed for easy protein tracking throughout purification. A more intense colour indicated a higher protein concentration but did not necessarily reflect purification quality (Figure 9). Proteins were purified and analyzed via SDS-PAGE to assess purity (Figure 10). Expression across gFlHb A, B, and E yielded 4-50 mg/L of culture, with no clear correlation between yield and assemblage type, although this may be a consequence of limited sample sizes.

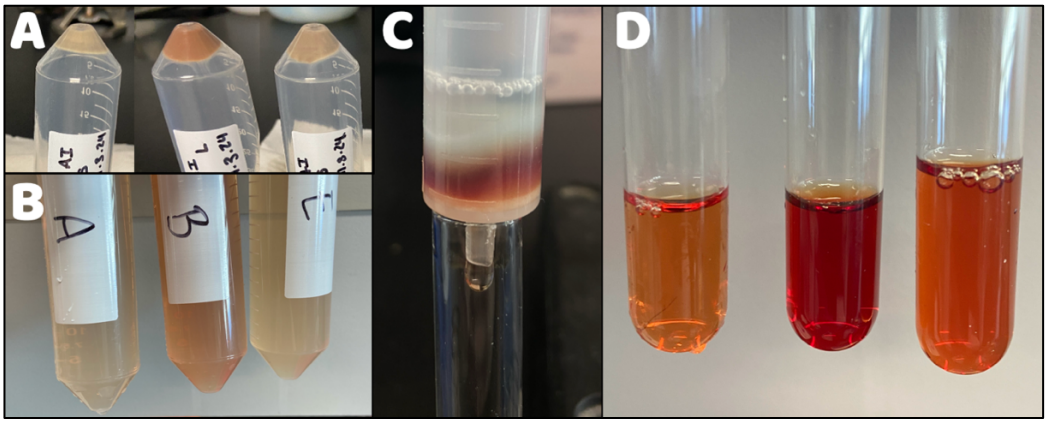

Figure 9: Images of protein samples at various purification stages. **(A)** *E. coli* cell pellets following expression. **(B)** Supernatants after cell lysis. **(C)** gFlHb B eluting from the Ni-NTA column. **(D)** Proteins post-desalting. In panels A, B, and D, gFlHb A, B, and E are arranged from left to right, with redder samples indicating a higher heme protein concentration.

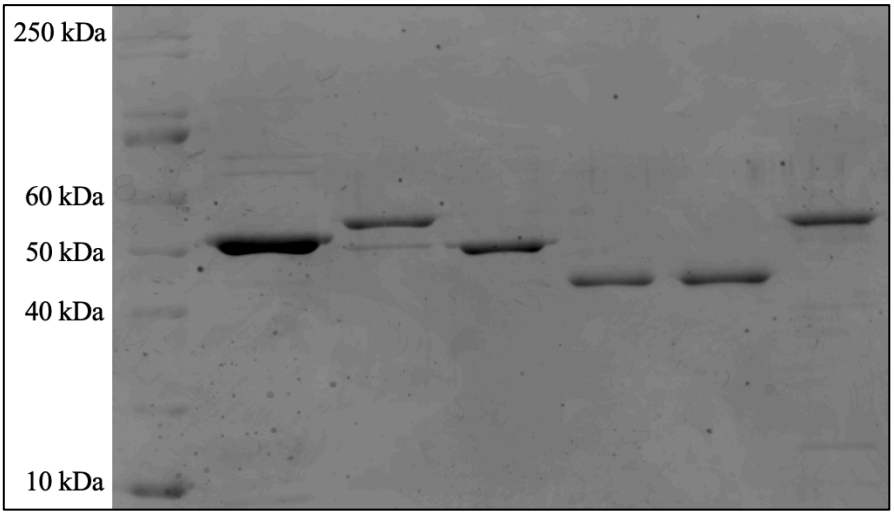

Figure 10*: SDS-PAGE gel stained with Coomassie Brilliant blue: lane 1, size ladder (NEB #P7704, 10-250 kDa); lane 2, glFHb A; lane 3, gFlHb B; lane 4, gFlHb E; lane 5, Hmp (no shoulder); lane 6, Hmp (shoulder); lane 7, gFlHb A W90A/M299A.*

Occasionally, deviations in spectral properties were observed including a right-shifted 'shoulder' peak alongside the Soret peak (Figure 11). This feature persisted across purification stages, suggesting an expression-related rather than purification-induced artifact. Variations in incubation time, temperature, and shaking speed did not consistently influence its occurrence. The shoulder near 430 nm corresponds to the absorbance maximum of the reduced-deoxygenated species, which is unexpected under

oxidizing conditions where the protein is expected to be entirely in the ferric (Fe^{3+}) state. The shoulder persisted when potassium ferricyanide was added as an additional oxidizing agent. Protein preparations, both Hmp and gFlHb A have been found to possess this shoulder, though its occurrence remains a mystery.

Typically, flavohemoglobins exist in an equilibrium between different heme states, including the ferric (Fe^{3+}), ferrous (Fe^{2+})-oxygenated, and ferrous-deoxygenated states.[62] A peak near 430 nm can be associated with a five-coordinate high-spin ferrous species, where the heme iron is not fully occupied by a strong ligand, such as oxygen or nitric oxide.[33] Given that experimental conditions are aerobic, favouring the ferric state, the persistence of this shoulder suggests that another ligand may be competing for binding, that structural constraints are preventing full oxygen binding, or that the heme group itself has been altered. Heme extraction and mass spectrometry would be valuable in identifying the nature of this species.

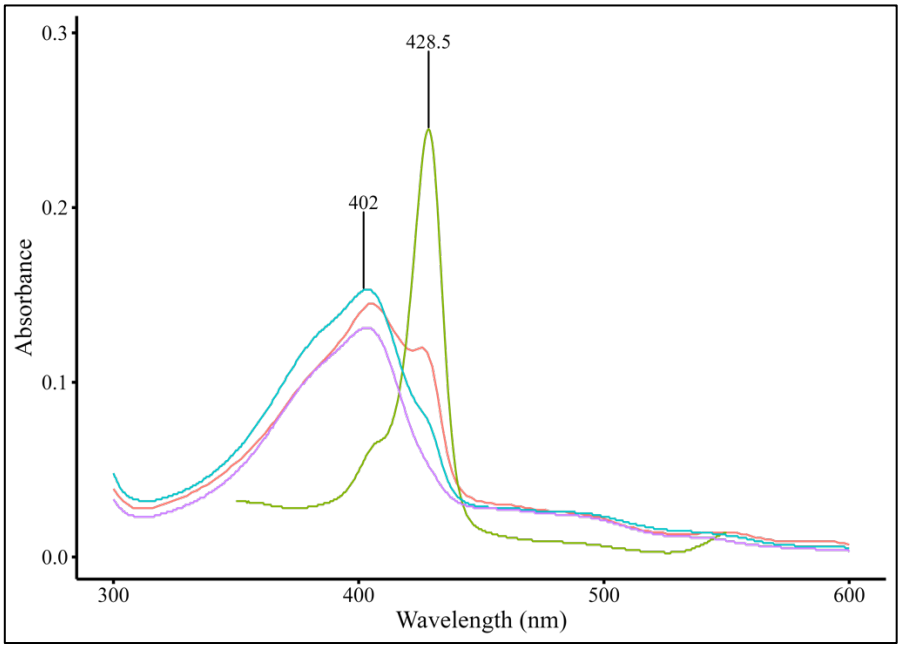

Figure 11: Spectra showing the Soret peak (402-407 nm) and the anomalous 'shoulder' (428.5 nm). Different colours represent different protein preparations: green (predominantly shouldered), purple (non-shouldered), and blue/pink (intermediate states).

Kinetic comparison among assemblages revealed minor differences in NADH oxidase activities (Figure 12). No significant difference was observed between gFlHb A and B ($P = 0.018$), while gFlHb E showed significantly different activity compared to gFlHb A and B ($P < 0.0001$) (Table 5). The box plot represents a range of specific activities across the three assemblages. The shaded boxes indicate the interquartile range (IQR), where 50% of the data points are concentrated, while the tails extend to the minimum and maximum values within 1.5 times the IQR. Shorter tails suggest lower variability in the dataset. Outliers, shown as individual points, were identified using the IQR rule, where any values beyond 1.5 x IQR from either side of the shaded box were excluded.

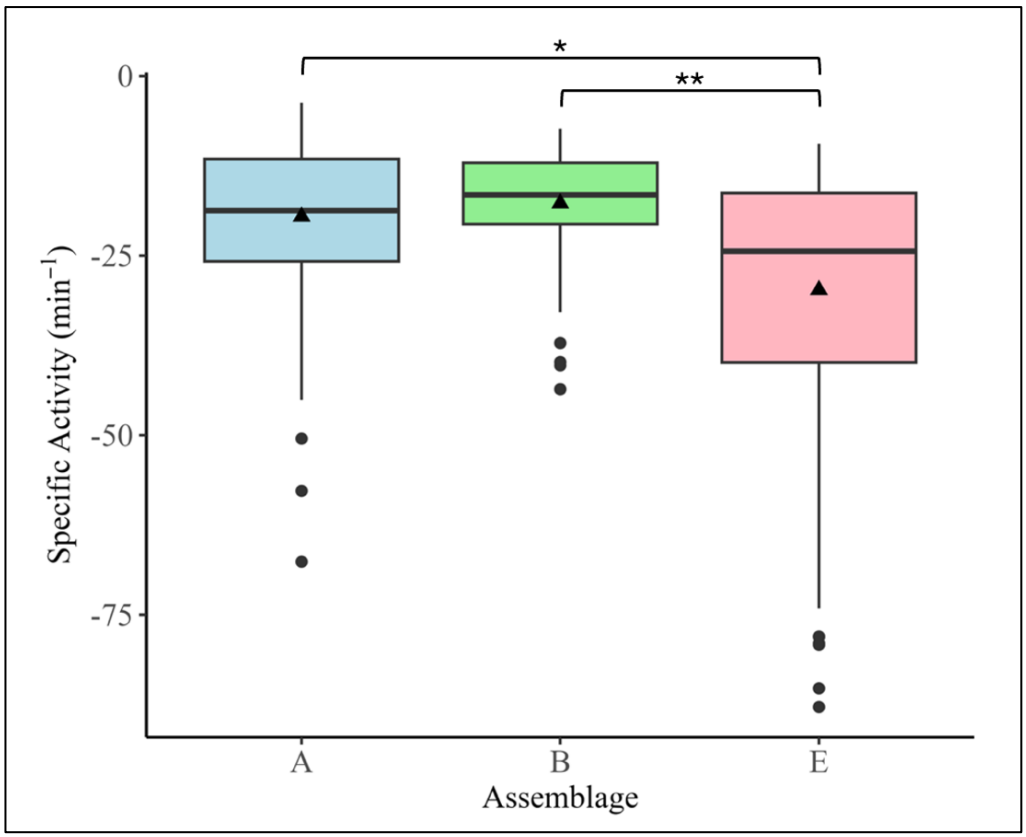

Figure 12: Box plot of NADH oxidase specific activity distributions for gFlHb A (blue), B (green), and E (pink). Horizontal black lines denote medians, ▲ represent means, and ● indicate outliers, as determined by the IQR rule. *corresponds to a difference in means of 10.2 min^{-1} and **corresponds to a difference of 12.1 min^{-1}.

Table 5: Average specific activities of gFlHb A, B, and E with standard deviations and 95% confidence intervals (n = 462, 202, 159 for gFlHb A, B, and E, respectively).

Assemblage	Average specific activity (min^{-1})	95% confidence interval
gFlHb A	-19.6 ± 9.7	-20.4, -18.7
gFlHb B	-17.7 ± 6.9	-18.7, -16.8
gFlHb E	-29.8 ± 13.4	-32.5, -27.0

Given that gFlHb E is more often associated with livestock rather than humans, its higher NADH oxidase activity may reflect adaptations to distinct host environments, where differences in oxidative stress could drive selective pressures on flavohemoglobin function. Livestock, particularly ruminants, host a more complex microbiota than humans due to their reliance on microbial fermentation for plant digestion.[63] Since ruminants lack the enzymatic machinery to break down plant fibers, they depend on symbiotic microorganisms to degrade plant polymers and generate usable nutrients.[63] This fermentation process produces various metabolic byproducts, and the high microbial activity required for continuous fermentation can increase reactive oxygen species production, potentially contributing to oxidative stress in the livestock gut.[64]

In this context, the higher NADH oxidase activity observed in gFlHb E may represent an evolutionary adaptation that enhances Giardia's ability to survive in these oxidative conditions. However, despite the statistical significance of the NADH oxidase activities, the biological relevance remains questionable. The mean specific activity differences are -10.2 min^{-1} (gFlHb E vs. A) and -12.1 min^{-1} (gFlHb E vs B). While the *P* values indicate significance, these differences are small relative to the intrinsic variability observed within each assemblage. When outliers are excluded, the NADH oxidase activity of

gFlHb A can range from -5 to -45 min^{-1}. The box plot also shows substantial overlap between the assemblages, suggesting that the observed differences may not reflect a functionally significant divergence (Figure 12). While oxidative stress mitigation is likely under selective pressure in the livestock gut, gFlHb may not be the primary contributor to this adaptation.

FAD dependence varied among assemblages, with gFlHb A showing the highest sensitivity, plateauing at higher FAD concentrations, while gFlHb B had the highest affinity, saturating at lower FAD levels (Figure 13). These differences suggest variations in flavin binding affinity that could influence electron transfer efficiency during redox reactions. gFlHb A and E's higher sensitivities may indicate a greater reliance on intracellular FAD levels, potentially allowing for dynamic regulation of activity. In contrast, gFlHb B, which saturates at lower concentrations of FAD, may have evolved to function efficiently in environments where FAD availability is more limited.

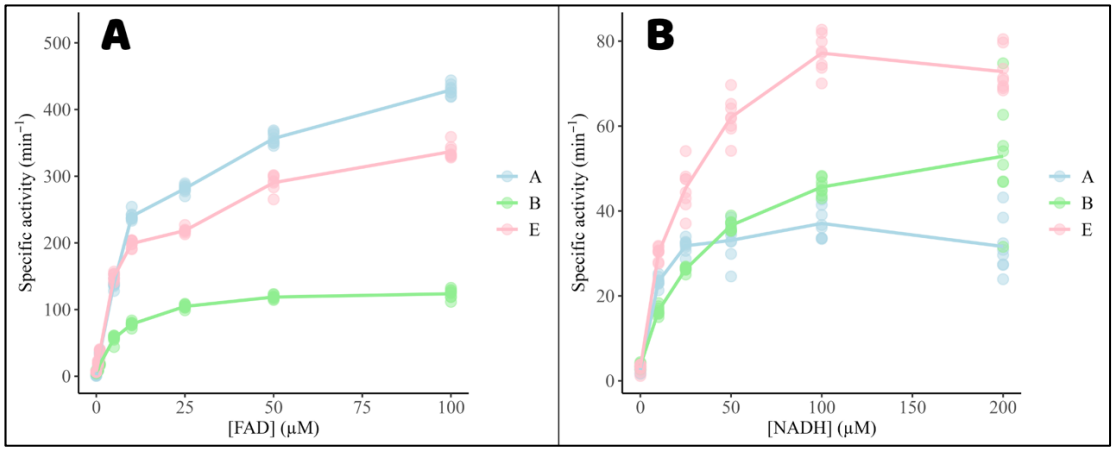

Figure 13: FAD **(A)** and NADH **(B)** dependence of assemblage A (blue), B (green), and E (pink). Assays were run at 37°C in 100 mM Bis-Tris buffer (pH 6.5). **(A)** 100 µM NADH, 1 µM gFlHb, variable FAD concentrations. **(B)** 1 µM FAD, 0.1 µM gFlHb, variable NADH concentrations.

Variations in the NADH oxidase activity of one assemblage may stem from differences in endogenous FAD levels. Since this activity is highly FAD-dependent, the absence of exogenous FAD substantially reduces activity (Table 6). However, some activity persists due to endogenous FAD within the proteins. Enzyme preparations with higher heme-to-FAD ratios, indicating higher heme concentrations relative to FAD have a lower NADH oxidase activity (Table 7). In other words, proteins with higher endogenous FAD concentrations maintain greater NADH oxidase activity regardless of exogenous FAD availability.

Table 6: Effects of exogenous FAD on the NADH oxidase specific activity of different gFlHb A, B, and E preparations.

gFlHb prep	Specific activity + 1 µM FAD (min^{-1})	Specific activity no added FAD (min^{-1})
A1	-10.7 ± 0.5	-2.5 ± 0.3
A2	-25.3 ± 2.5	-2.2 ± 0.3
A3	-6.8 ± 0.2	-3.2 ± 0.3
B1	-12.3 ± 0.9	-4.4 ± 0.3
E1	-11.8 ± 0.6	-1.6 ± 0.3

Table 7: Heme to endogenous FAD concentration and NADH oxidase specific activity to endogenous FAD concentration ratios of different gFlHb B preparations.

gFlHb prep	Heme: FAD	Specific activity (min^{-1})
gFlHb B1	0.8	-6.590 ± 0.97
gFlHb B2	1.1	-4.674 ± 0.70
gFlHb B3	1.0	-4.826 ± 0.58

NADH dependence analysis confirmed saturation below 100 μM, with K_m values of 10 μM, 32 μM, and 16 μM for gFlHb A, B, and E, respectively (Figure 13). These differences suggest that gFlHb A has the highest affinity for NADH, reaching saturation at a lower concentration, while gFlHb B and E require more NADH to achieve maximal activity. A higher NADH affinity may allow gFlHb A to function efficiently under conditions of limited NADH availability, while gFlHb B and E may depend on a more abundant NADH pool to maintain their activity. A saturating concentration of NADH (100 μM) was included in NADH oxidase reactions to account for this variability.

In terms of their amino acid sequences, gFlHb A, B, and E are highly similar, sharing at least 70% sequence identities with one another (Table 8). All three assemblages have the unique sequence inserts not found in other flavohemoglobins, and even when residues are not identical, substitutions between the assemblages are mostly conservative, trading one basic residue for another, for example (Figure 14). Despite this overall similarity, key differences in specific residues could contribute to variations in structural stability, enzymatic activity, or interactions with ligands and cofactors. Additionally, differences (or similarities) could be exploited if gFlHb is considered as a drug target.

Table 8: Sequence identities between gFlHb A, B, and E, calculated via UniProt.

gFlHb	Sequence identity (%)
A–B	71.3
A–E	86.6
B–E	74.8

Figure 14: Sequence alignment of gFlHb A, B, E1, and E2. The sequence inserts are highlighted in cyan (globin domain) and orange (FNR domain). Asterisks indicate identical residues, while colons and periods indicated similar residues.

Giardia assemblage E contains two forms of gFlHb, E1 and E2 which differ only by six residues (Table 9). Although most of the substitutions are conservative, gFlHb E1 has S66, a small, polar amino acid and gFlHb E2 has P66, a larger, cyclic, non-polar amino acid. This may affect hydrogen bonding and overall protein folding, though one substitution is unlikely to interrupt the overall fold of gFlHb. The substitution does not occur in either the active site or the NADH-binding site. The change from V43 to I43

does occur within the active site, however this is a conservative substitution where one non-polar uncharged amino acid is switched for another. The substitutions at residues 82, 135, 286, and 298 also do not occur in the active or NADH-binding sites. Because of the miniscule differences, we chose only to study gFlHb E1.

Table 9: Non-conserved residues between gFlHb E1 (UniProt #E1F8Q4) and E2 (#E1F8H4).

Residue	gFlHb E1	gFlHb E2	Effect
43	V	I	Conservative substitution
66	S	P	May disrupt protein folding
82	A	T	T may introduce a hydrogen bond
135	R	K	Conservative substitution
286	A	T	T may introduce a hydrogen bond
298	V	M	Conservative substitution

Residue analysis of the NADH-binding and active sites revealed a high degree of conservation among gFlHb A, B, and E, with a few notable differences (Table 10). gFlHb B contains four additional residues within the NADH-binding site, which could influence its binding affinity. gFlHb B has a higher K_m value (32 μM) than gFlHb A (10 μM), indicating a lower affinity for NADH. These additional residues may introduce steric hinderance, modify the electrostatic environment, and alter the conformation of the NADH-binding pocket potentially weakening NADH interactions.

Structural predictions suggest that the nicotinamide ring of NADH in gFlHb B faces the opposite direction compared to gFlHb A and E, possibly allowing it to interact with these extra residues (Figure 15). This altered positioning could either reduce NADH binding affinity by disrupting optimal interactions within the pocket or, conversely, increase affinity by creating new interactions. However, the higher K_m value of gFlHb B

suggests that the former scenario is more likely. As this observation is based on a predicted model rather than experimental data, structural studies are required for validation.

In the active site, I43 (gFlHb A) is replaced by V43 (gFlHb B and E), a conservative substitution that, despite the similar properties of these residues, could still impact enzyme efficiency or heme positioning due to the smaller side chain of valine. Another key difference is the orientation of R53, which is inward-facing in gFlHb A but outward-facing in gFlHb B and E. This variation could influence the electrostatic environment of the heme pocket. Since arginine carries a positive charge at physiological pH, an inward-facing R53 in gFlHb A may interact with the negatively charged propionate groups of heme, stabilizing its position within the active site (Figure 16). This stabilization could influence heme binding affinity, potentially affecting its redox properties or ligand accessibility. In contrast, an outward-facing R53 may weaken these stabilizing interactions, leading to a more flexible heme environment that could alter electron transfer dynamics or ligand coordination. Structural mutations to R53 would help determine whether this difference contributes to heme stability and reactivity.

Table 10: Non-conserved residues in the NADH-binding site and active sites of gFlHb A, B, and E. Refer to appendix (Table A1) for an exhaustive list of conserved residues in the binding sites.

Assemblage	Residues in the NADH binding site	Residues in the heme-binding active site
gFlHb A	I322, A351	I43, R53 (inward)
gFlHb B	D248, M429, E449, M450, F451	V43, R53 (outward)
gFlHb E	A350, A351, A430	V43, R53 (outward)

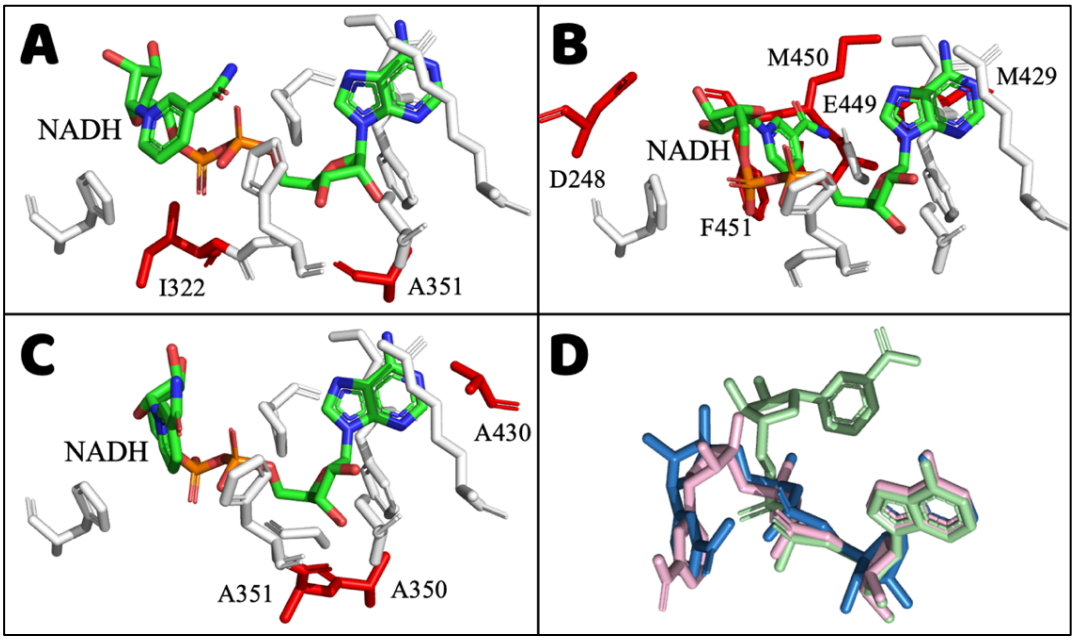

Figure 15: Conserved residues in the NADH binding sites of gFlHb A **(A)**, gFlHb B **(B)**, and gFlHb E **(C)** are pictured in white and non-conserved residues are pictured in red. **(D)** An overlay of NADH in gFlHb A (blue), gFlHb B (green), and gFlHb E (pink) where gFlHb B is oriented in the opposite direction.

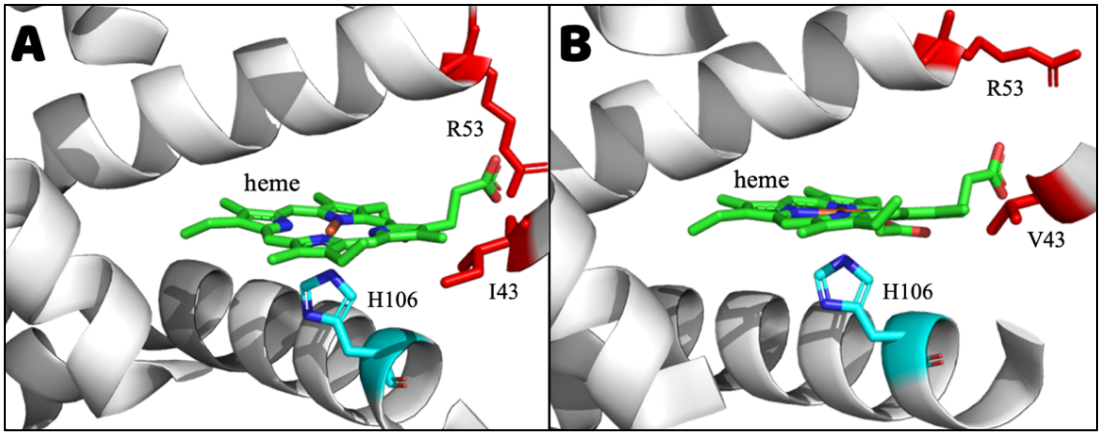

Figure 16: Non-conserved residues in the heme-binding active site (pictured in red) in gFlHb A **(A)** compared to gFlHb B and E **(B)**. I43 (gFlHb A) is substituted with the smaller V43 (gFlHb B, E), and R53 is pointed inwards (gFlHb A) versus outwards (gFlHb B, E).

3.3. Inhibition of gFlHb

To investigate the role of the heme group in NADH oxidase activity, flavohemoglobin inhibitors were introduced. Imidazole-based compounds, with their bulky aromatic substituents, selectively and strongly inhibit nitric oxide dioxygenase activity by fitting into the hydrophobic pocket and coordinating with the heme.[41] Imidazole can donate lone pairs of electrons from its nitrogen atom to the iron center of the heme, forming a ligand-metal bond. This allows imidazole to mimic natural ligands such as nitric oxide and oxygen, binding to the active site in place of these molecules and disrupting the flavohemoglobin's nitric oxide dioxygenase activity. Additionally, imidazole-based compounds can sterically hinder substrate access and alter the heme environment, further inhibiting enzyme function. Imidazole, miconazole, nitrite, and cyanide were studied in this thesis, with concentrations chosen based on a previous study.[58] While these inhibitors are typically studied in the context of drug targeting, their impact on NADH oxidase activity of gFlHb may provide insight into electron transfer pathways in the absence of nitric oxide.

Imidazole, nitrite, and miconazole showed no change in NADH oxidase activities for gFlHb A, B, and E (Table 11), suggesting that their binding does not interfere with enzyme turnover. In contrast, cyanide resulted in activity reductions that exceeded the standard deviation in all three assemblages, with percent decreases of 44.6%, 56.4%, and 44.3% for gFlHb A, B, and E, respectively. These experiments were conducted without the addition of FAD to avoid the possibility of electrons being diverted through alternative pathways, such as onto the exogenous FAD. Our goal was to minimize the risk

of electrons being redirected, thereby maintaining physiological conditions as closely as possible to study the true path of electrons.

Table 11: Effect of inhibition on the NADH oxidase activity of gFlHb A, B, and E. The average of 15 replicates was reported for each condition, with their associated standard deviations.

	Specific activities (min^{-1})		
Inhibitors	**gFlHb A**	**gFlHb B**	**gFlHb E**
none	-1.9 ± 0.4	-3.9 ± 0.8	-1.6 ± 0.2
1 mM imidazole	-1.8 ± 0.4	-3.8 ± 0.9	-1.6 ± 0.2
1 mM nitrite	-1.9 ± 0.5	-3.7 ± 0.9	-1.6 ± 0.2
DMSO control	-2.0 ± 0.3	-2.9 ± 1.0	-1.5 ± 0.2
20 μM miconazole	-1.9 ± 0.3	-2.8 ± 0.8	-1.5 ± 0.2
1 mM cyanide	-1.1 ± 0.4	-1.2 ± 0.3	-0.8 ± 0.2

During the reaction cycle of flavohemoglobins the heme iron cycles between at least three distinct states: ferric (Fe^{3+}), also called oxidized; deoxygenated (Fe^{2+}); and oxygenated (Fe^{2+}–O_2) (Figure 17). The oxidized state represents the resting form of the heme, while reduction with NADH in the presence of molecular oxygen generates the reduced-oxygenated state and treatment with sodium dithionite produces the reduced-deoxygenated state, as it not only reduces heme, but also consumes oxygen in solution. Addition of exogenous ligands such as imidazole, nitrite, miconazole, and cyanide to gFlHb caused optical shifts that indicated ligand binding to the oxidized state (Figure 18).

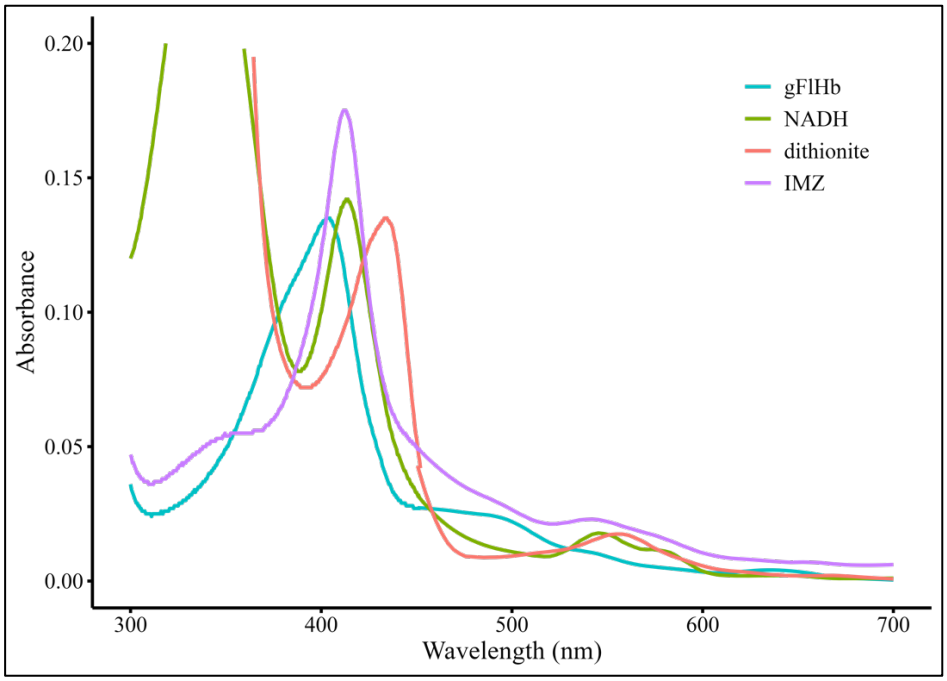

Figure 17: UV-Visible spectra of gFlHb A in different oxidation and ligation states: ferric (gFlHb; blue), oxygenated (NADH; green), deoxygenated state (dithionite; red), and ferric-imidazole complex (IMZ; purple). 1 µM gFlHb was mixed with 100 µM NADH, 10 mM sodium dithionite, or 1 mM imidazole.

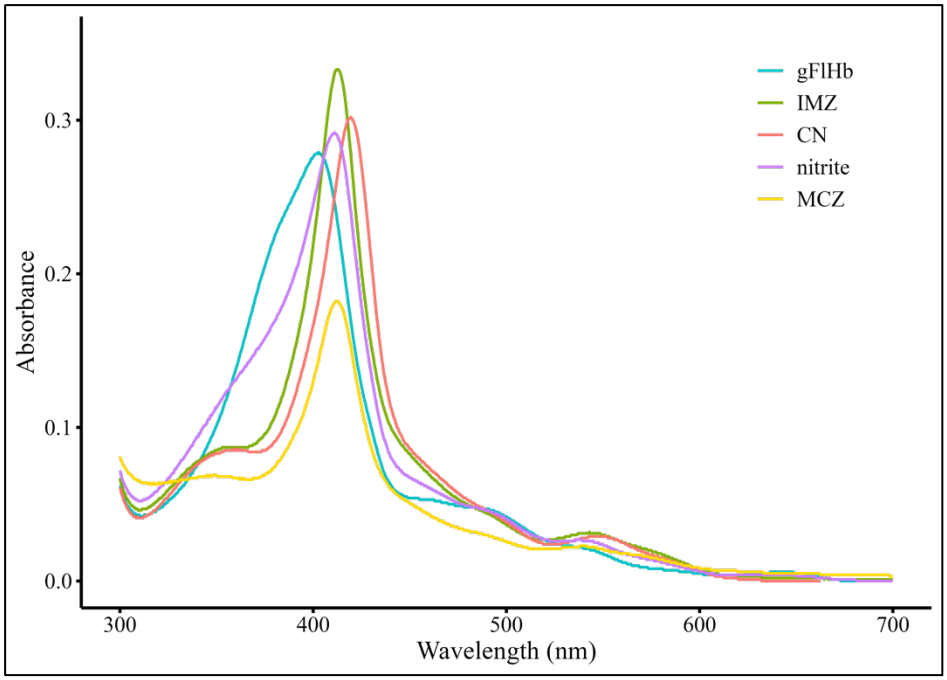

Figure 18: UV-visible spectra of 2 µM ferric gFlHb A with different exogenous ligands and their associated absorbance maxima, (λ_{max}). Blue, no added ligand (λ_{max} 402 nm); green, 1 mM imidazole (λ_{max} 413 nm); red, 1 mM cyanide (λ_{max} 420 nm); purple, 1 mM nitrite (λ_{max} 411 nm); yellow, 20 µM miconazole (λ_{max} 413 nm).

Blocking access to the heme group does not appear to interfere with oxygen binding. For example, when imidazole was added, followed by NADH, the reduced-oxygenated iron still formed, as indicated by the Q peaks especially (500-600 nm). This was observed for imidazole, nitrite and miconazole, demonstrating that the presence of inhibitors does not impair the transition between heme states or oxygen binding (Figure 19). However, the two peaks present at 545 nm and 580 nm are not as pronounced when cyanide is present. This suggests that cyanide blocks the binding of oxygen, as an optical shift occurs. Since NADH oxidase activity depends on oxygen binding, these data further support the conclusion that imidazole, nitrite and miconazole do not disrupt this enzyme function, though they do inhibit the nitric oxide dioxygenase activity to varying degrees,[59] and that cyanide does decrease activity.

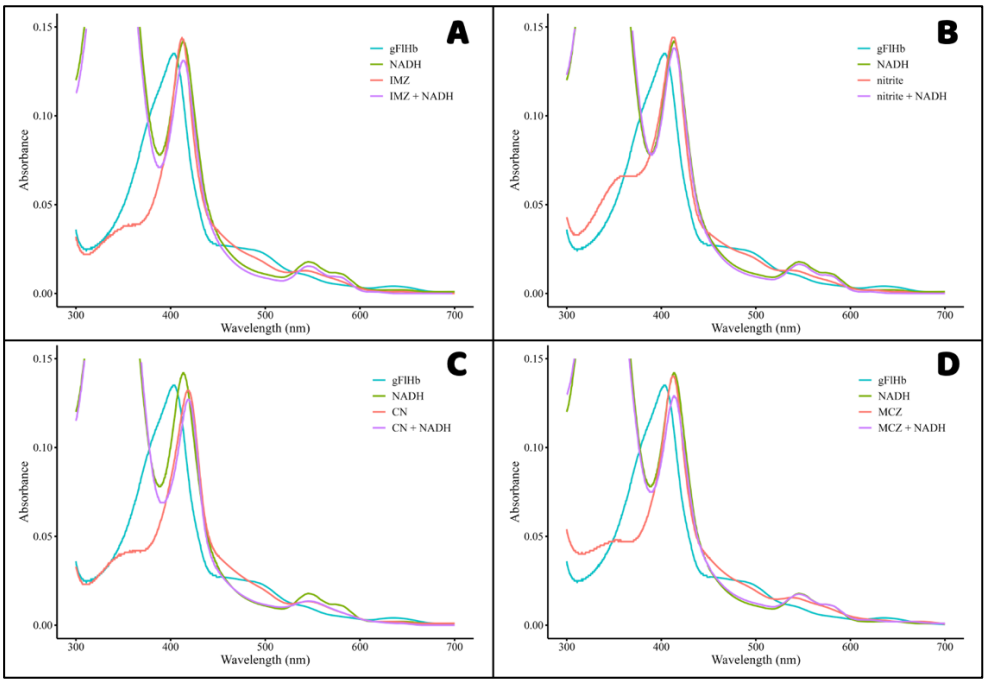

Figure 19: Spectra of 1 µM gFlHb A in ferric and oxygenated states in the presence of 1 mM imidazole **(A)**, 1 mM sodium nitrite **(B)**, 1 mM sodium cyanide **(C)**, and 20 µM miconazole **(D)**. Spectra in each panel are coloured as follows: blue, ferric enzyme without added ligand; green, oxygenated enzyme without added ligand; red, ferric enzyme with added ligand; and purple, oxygenated enzyme with added ligand. Where present, the oxygenated state was formed by the addition of 100 µM NADH under aerobic conditions.

Binding to the reduced-deoxygenated state of the protein, achieved by the addition of sodium dithionite, was not observed with imidazole, only partially observed with nitrite and miconazole, and fully observed with cyanide (Figure 20). This is shown by the absence of optical changes between the dithionite and dithionite + imidazole spectra (Figure 20A), compared to the clear shift observed when cyanide binds in the reduced-deoxygenated state (Figure 20C).

Cyanide exhibited the strongest binding affinity for both the oxidized and reduced iron states, with a K_D of 10 ± 2 μM,[65] likely due to its small size and high reactivity. Unlike imidazole, miconazole, and nitrite which have K_i values of 20 ± 6, 10 ± 2, and 32 ± 12 μM,[59] respectively, cyanide was the only compound that noticeably decreased the NADH oxidase activity in gFlHb A, B, and E, suggesting a more direct impact on electron transfer. Previous studies show that cyanide remains bound to iron in both oxidation states. Cox and Hollaway (1977) reported the formation of a transient Fe(II)-CN complex in myoglobin upon reduction of Fe(III)-CN, suggesting that cyanide binding persists, at least temporarily.[66] Future work should include additional measurements of the Fe(II)-CN complex at later time points than reported here (Figure 20) to determine the stability of this intermediate. In contrast, there is no direct evidence for the formation of a Fe(II)-imidazole intermediate.[66] Similarly, Yoshikawa and Caughey (1990) provided further evidence for cyanide binding to both the reduced and oxidized iron states.[67] Although the nearby copper center in cytochrome *c* oxidase may influence this binding. Studies on different myoglobin isotypes revealed that *A. limacina* myoglobin had the slowest cyanide dissociation rate after the dithionite addition, potentially due to the stabilizing arginine (helix E) in the distal heme pocket, rather than the distal histidine

typically found in globin proteins.[68] Together, these findings support the ability of gFlHb to bind cyanide in both oxidations states, reinforcing its potency as an inhibitor.

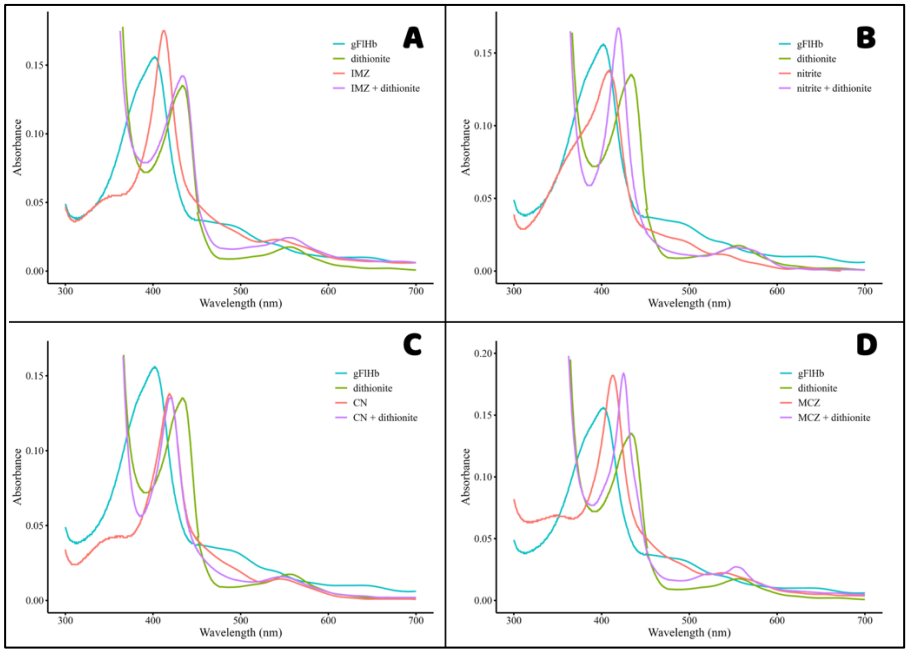

Figure 20: Spectra of 1 µM gFlHb A in ferric and deoxygenated states in the presence of 1 mM imidazole **(A)**, 1 mM sodium nitrite **(B)**, 1 mM sodium cyanide **(C)**, or 20 µM miconazole **(D)**. Spectra in each panel are coloured as follows: blue, ferric enzyme without added ligand; green, deoxygenated enzyme without added ligand; red, ferric enzyme with added ligand; purple, deoxygenated enzyme with added ligand. Where present the deoxygenated state was formed by the addition of 10 mM sodium dithionite under anaerobic conditions.

Although flavohemoglobins are not currently considered drug targets for giardiasis due to the difficulty of knocking down the gFlHb gene, future studies could focus on identifying inhibitors as potent as cyanide, but significantly less toxic. Isocyanide complexes, such as Xanthocillin, are being investigated for their antimicrobial potency, particularly against bacterial cells.[69] These compounds target the iron within the heme group, leading to the accumulation of reactive oxygen species and subsequent cell destruction.[70] While promising, Xanthocillin has been shown to kill *E. coli*, a non-desirable consequence given its role as a beneficial gut bacterium. As an alternative approach, inhibitors could be designed to disrupt electron transfer pathways without

directly binding them heme group. For instance, menadione (vitamin K3) has been proposed as a potential candidate for interfering with redox balance in pathogens.[71]

3.4. Lipid interactions with gFlHb

Flavohemoglobins are known to bind fatty acids and phospholipids, and several techniques have been used to remove lipids from purified proteins. Lipid removal was attempted by passing the proteins through three different chromatography resins: ceramic hydroxyapatite (CHT), Sephadex LH-20, and hydroxylalkoxypropyl dextran. These are collectively referred to as lipidex columns, and they are designed to remove lipids by allowing 'lipid-free' proteins to pass through. The effectiveness of these resins was assessed by thin-layer chromatography (TLC) of organic solvent extracts of flavohemoglobins that had been run through one of these columns, optimized using a 3:2 hexane: ethyl acetate solvent ratio, where clear separation was achieved (Figure 21).

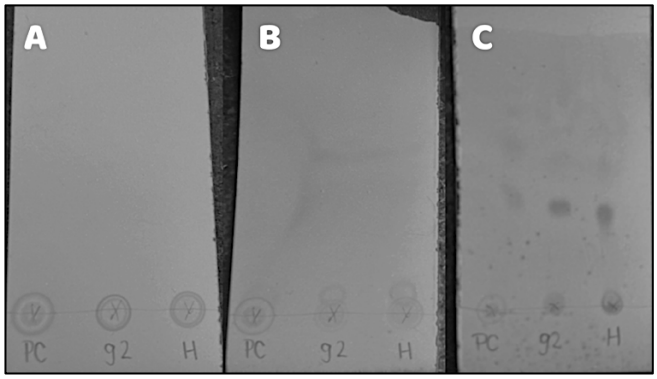

Figure 21: Solvent optimization for lipid TLC. Plates were exposed to iodine vapour and imaged with UV light before **(A)** and after running with a 2:1 **(B)** and 3:2 **(C)** hexane: ethyl acetate solvent system. In all panels, phosphatidylcholine (PC; phospholipid control), gFlHb A (g2), and Hmp (H) were spotted.

If the lipidex columns were effective in separating lipids from the protein samples, we would not expect to see lipid spots on the TLC plate. However, lipid extracts from proteins passed through none, one, or all these columns still showed spots with retention

factors (the ratio of the distance travelled by the sample to the solvent front) identical to those of our lipid controls (Figure 22A). Despite the columns not removing the lipids as expected, the samples were further analyzed using ESI mass spectrometry, where the same major peaks were observed for each sample, in similar abundances (Table A2).

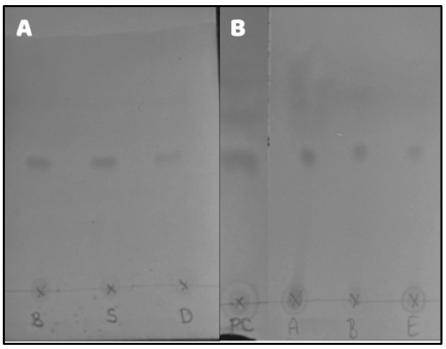

Figure 22: (A) TLC plate with lipid extracts of gFlHb A before any columns (B), after the Sephadex LH-20 column (S) and after Sephadex, CHT, and hydroxylalkoxypropyl columns (D). **(B)** Lipid extracts of gFlHb A, B, and E with a phosphatidylcholine (PC) control. TLC was run in 3:2 hexane: ethyl acetate and imaged under UV light after exposure to iodine vapour.

These challenges in lipid removal are common, as some proteins bind strongly to lipids, which may be essential for their function. For instance, lipids are known to facilitate the clustering of kinases and receptors to initiate immune signalling during allergic reactions.[72] Similarly, certain proteins contain hydrophobic cavities that sequester lipids, potentially preventing lipid-protein complexes from being exposed to the lipidex matrices and thus hindering their removal during purification.[73] Based on the results presented, gFlHb appears to have a complex relationship with lipids that is not easily disrupted by conventional purification methods. However, this observation contrasts with findings for Hmp, where proteins passed through hydroxylalkoxypropyl dextran and CHT columns are classified as 'lipid-free'.[43,74,75]

Typically, when ligands bind to the heme group of proteins, optical changes can be observed, as seen with inhibitors. A similar optical shift occurs in Hmp upon binding

linoleic acid, a fatty acid, where a broad, asymmetrical Soret peak at 403 nm transitions to a sharp, symmetric peak at 407 nm.[75] Although optical changes were difficult to interpret due to ethanol-induced shifts, a subtle rightward shift in the Soret peak of gFlHb was still observed with the addition of linoleic acid (Figure 23). This suggests that linoleic acid interacts with gFlHb, even in the presence of ethanol, which is used as a cosolvent to solubilize the linoleic acid. D'Angelo et al. (2004) interpret the broad, asymmetric peak as a marker for the 'lipid-free' species. However, our observations suggest that this peak may indicate the presence of bound lipids, as we observe it even in proteins not passed through lipidex columns. This raises the possibility that the 'lipid-free' species may, in fact, still contain lipids, or alternatively, the samples may never have contained lipids to begin with. TLC analyses, which did not show differences between 'lipid-free', and 'lipid-containing' extracts, could support either possibility, though mass spectrometry supports the former, as non-solvent related peaks were detected in the expected ranges for fatty acids (100-300 m/z, $[M-H]^-$)[76] and phospholipids (600-900 m/z, ($[M-H]^-$).[77]

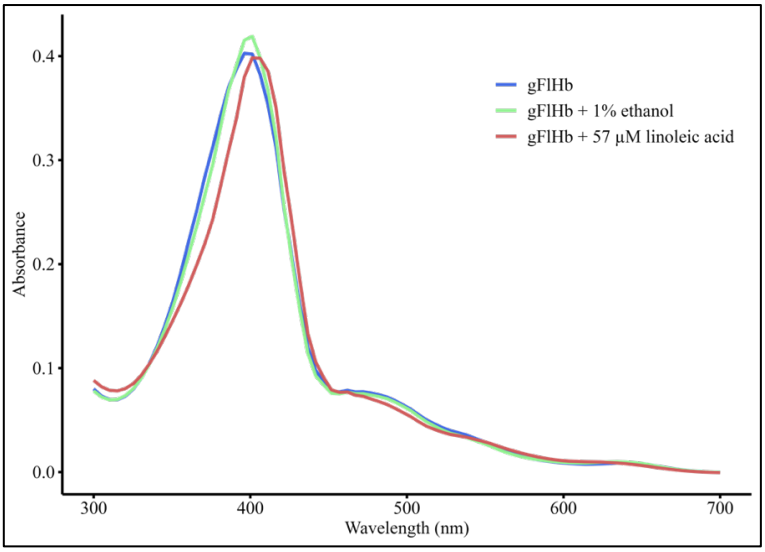

Figure 23: Optical changes induced by linoleic acid binding to gFlHb A. A slight shift to the right is observed with the addition of linoleic acid (green), while gFlHb (blue) and ethanol (red) show different spectral characteristics.

Lipid extracts from gFlHb A, B, and E were analyzed using TLC, revealing similar spots across all samples, including the phospholipid control (Figure 22). Due to the polarity of the compounds, the spots migrated up the plate with a relatively non-polar solvent, suggesting that the observed spots are likely free fatty acids, rather than phospholipids, which would be expected near the point of sample application. However, spots near the application points appeared in all samples, indicating the presence of phospholipids or other polar lipids. ESI mass spectrometry confirmed this observation, with predominant peaks at 393.28 m/z in gFlHb A and 197.81 m/z in gFlHb B and E (Table A3). Lipidomic analysis using LipidMaps® identified minor peaks potentially corresponding to phosphatidylethanolamine and phosphatidylcholine in the $[M-3H]^{3-}$ state. A comparison of a phosphatidylethanolamine ($C_9H_{18}NO_8P$, 299.21 g/mol) spectra with gFlHb A lipid extracts revealed similar peaks at 298.1575, 299.1512, 300.1895, 301.1239, 302.0629, 303.1011, 304.2808, and 305.1889 m/z (Figure 24). Although their relative abundance varies, these peaks likely correspond to phospholipids, such as phosphatidylethanolamine.

These findings suggest that gFlHb may associate with lipids of bacterial origin, warranting further investigation into its role in lipid interactions and membrane dynamics in Giardia. Since Giardia trophozoites cannot synthesize phospholipids *de novo*, they likely rely on lipids from the medium or the host.[78] Given that BL21(DE3) *E. coli* cells, which are used for the expression of flavohemoglobin vectors, naturally produce phospholipids, gFlHb likely encounters these during expression. While phosphatidylcholine is primarily found in eukaryotic cells, phosphatidylethanolamine constitutes 70-80% of bacterial membrane lipids.[79] The phosphatidylethanolamine-like peaks in the mass spectra support its potential inclusion in the lipid extracts.

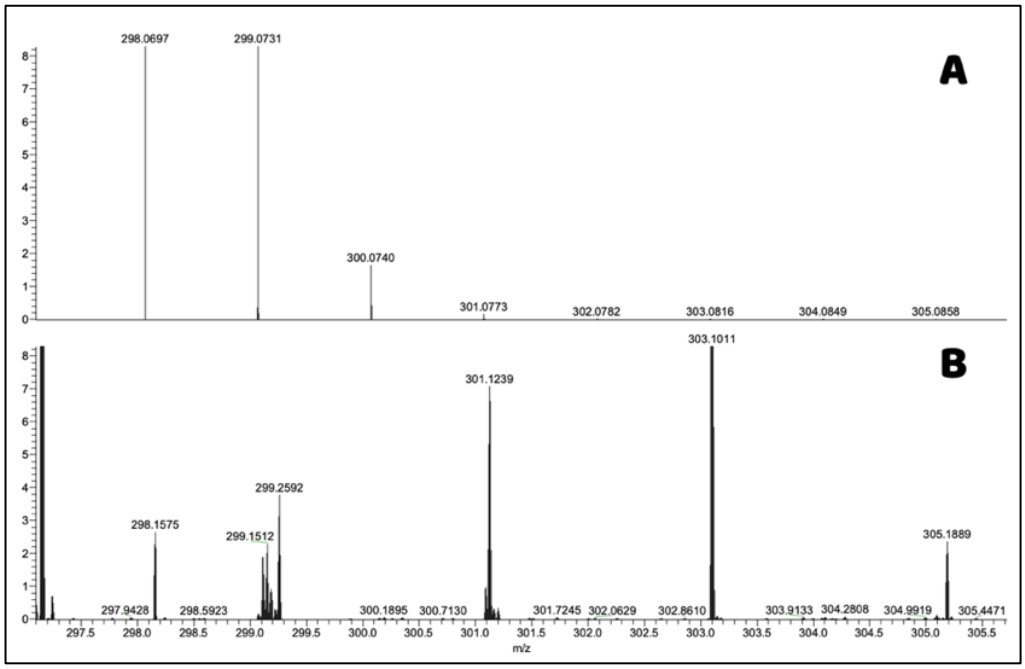

Figure 24: ESI-FTMS in negative ionization mode. **(A)** Phosphatidylethanolamine reference spectra ($C_9H_{18}NO_8P$). **(B)** gFlHb A lipid extract.

However, without prior knowledge of the lipid compositions in these samples, accurately identifying the species corresponding to the observed peaks remains challenging owing to variations in the chain length, the number of double bonds, and branching of fatty acids. While the detected signals fall within the expected range for lipids, further studies are needed for definitive identification. Mass spectrometry using known lipid standards, such as those characteristic of E. *coli* cells, could provide essential reference points for precise characterization.

Future experiments should focus on optimizing lipid removal from protein samples. This includes refining the use of the hydroxyapatite, LH-20 Sephadex, and hydroxylalkoxypropyl dextran columns. Although these resins were tested in this thesis, the limited sample sizes prevent us from definitively concluding that they are ineffective. If further optimization does not improve lipid removal, a phenyl-Sepharose column could

be used.[80] These resins have been used for lipid removal from fatty acid-binding proteins and could be optimized for the separation of flavohemoglobins and lipids. Additionally, analysis of the NADH oxidase activity before and after the removal of lipids would offer valuable insights into the functional significance of these lipid-protein interactions.

3.5. Implications of gFlHb in oxidative stress management

The addition of hydrogen peroxide to gFlHb A significantly increased its NADH oxidase activity from -17.7 min^{-1} to -51.9 min^{-1} ($t_{18.5}$ = 6.5388, $P < 0.0001$), corresponding to a 2.14–2.28-fold increase in activity with 95% confidence (Table 12). This increase in activity highlights gFlHb's potential to actively respond to oxidative stress by enhancing its function in the presence of hydrogen peroxide. In contrast, the NADH oxidase activity of Hmp was not stimulated by hydrogen peroxide ($t_{9.0}$ = -2.0176, P = 0.0744), suggesting a distinct functional difference between the two proteins in their response to oxidative conditions. This difference may reflect the differing antioxidant mechanisms employed by their respective host organisms. While Hmp contains superoxide dismutase, catalase, and glutathione peroxidase, Giardia lacks these conventional antioxidants, and instead possesses superoxide reductase and peroxiredoxins, less efficient enzymes in comparison.[21,22]

Table 12: NADH oxidase specific activities of gFlHb A and Hmp in the absence and presence of hydrogen peroxide.

	Specific activity (min^{-1})	
Assay	**gFlHb**	**Hmp**
NADH oxidase	-17.7 ± 6.9	-52.2 ± 7.9
NADH oxidase + 1 mM H_2O_2	-51.9 ± 21.5	-36.0 ± 7.4

Transcriptional upregulation of gFlHb A in the presence of 500 μM hydrogen peroxide (1.71-fold) and oxygen (7.16-fold), suggests that gFlHb may play a role beyond nitrosative stress regulation.[50] Given that nitric oxide also induces the expression of flavohemoglobins,[47] it is plausible that flavohemoglobins break down hydrogen peroxide, similarly to their role in nitric oxide detoxification. Under anaerobic conditions, Hmp acts as an alkyl hydroperoxide reductase, reducing these alkyl peroxides to their corresponding alcohols.[51,81] While Giardia likely does not experience a strictly anaerobic environment in the mammalian intestine, we aimed to determine whether gFlHb could also degrade hydrogen peroxide, but under aerobic conditions.

To investigate this, an HRP/ODA assay was used to measure hydrogen peroxide by monitoring the colorimetric shift in absorbance at 460 nm. The reaction, which relies on HRP-mediated oxidation of ODA in the presence of hydrogen peroxide, produces a red-coloured product. After allowing the NADH oxidase activity reaction to proceed until NADH depletion and then adding the HRP/ODA solution to test for interference, we unexpectedly observed a colour change, indicating hydrogen peroxide generation rather than consumption (Figure 25A). This colour change was prevented by the presence of catalase with gFlHb and NADH, confirming that the signal was due to hydrogen peroxide rather than other oxidants (Figure 25B). Additionally, a colour change was not observed when gFlHb was absent from solution (Figure 25C).

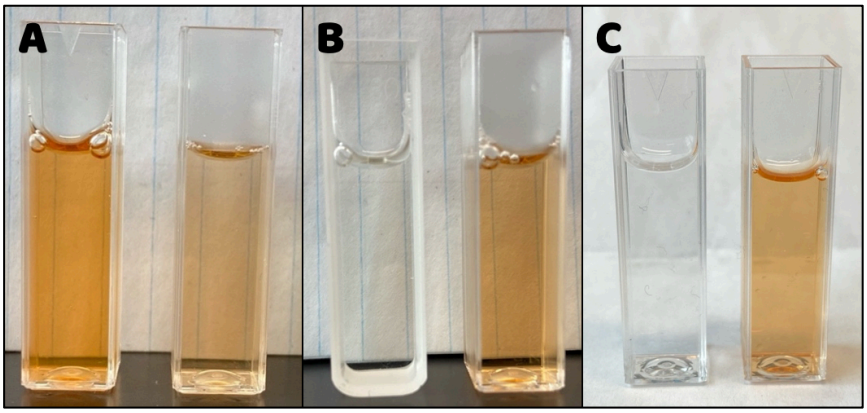

Figure 25: HRP/ODA assay, where all cuvettes contain 0.475 U/mL HRP and 0.1 mg/mL ODA in 100 mM Bis-Tris (pH 6.5). **(A)** The left cuvette has an added 0.1 mM H_2O_2, and the right cuvette contains 100 µM NADH, 1 µM FAD, and 1 µM gFlHb added to HRP/ODA after NADH oxidase reaction ran to completion. **(B)** Both cuvettes contain 100 µM NADH, 1 µM FAD, and 1 µM gFlHb. The left cuvette also contains 10 U/mL catalase. The reaction was run to completion before mixing with the ODA/HRP solution. **(C)** Assay with 100 µM NADH and 1 µM FAD after 10 minutes NADH oxidation without gFlHb (left) and with gFlHb (right).

Real-time monitoring of NADH consumption (A_{340}) and ODA oxidation (A_{460}) further validated the generation of hydrogen peroxide, with a clear increase in absorbance at 460 nm occurring after NADH was depleted, suggesting hydrogen peroxide is simultaneously produced with NADH consumption (Figure 26). However, due to NADH interference with the ODA assay (Figure 27), a more precise detection method is required for better quantification of hydrogen peroxide. This interference explains why the A_{460} did not change until NADH was almost entirely depleted, and why a less intense colour change was observed in its presence. Interestingly, the rate of NADH oxidation was faster after the second NADH addition, which is consistent with previous results that show hydrogen peroxide stimulating the NADH oxidase activity (Table 12). Moreover, after the third addition, the rate then slows down, aligning with the heme breakdown observation (Figure 29-32).

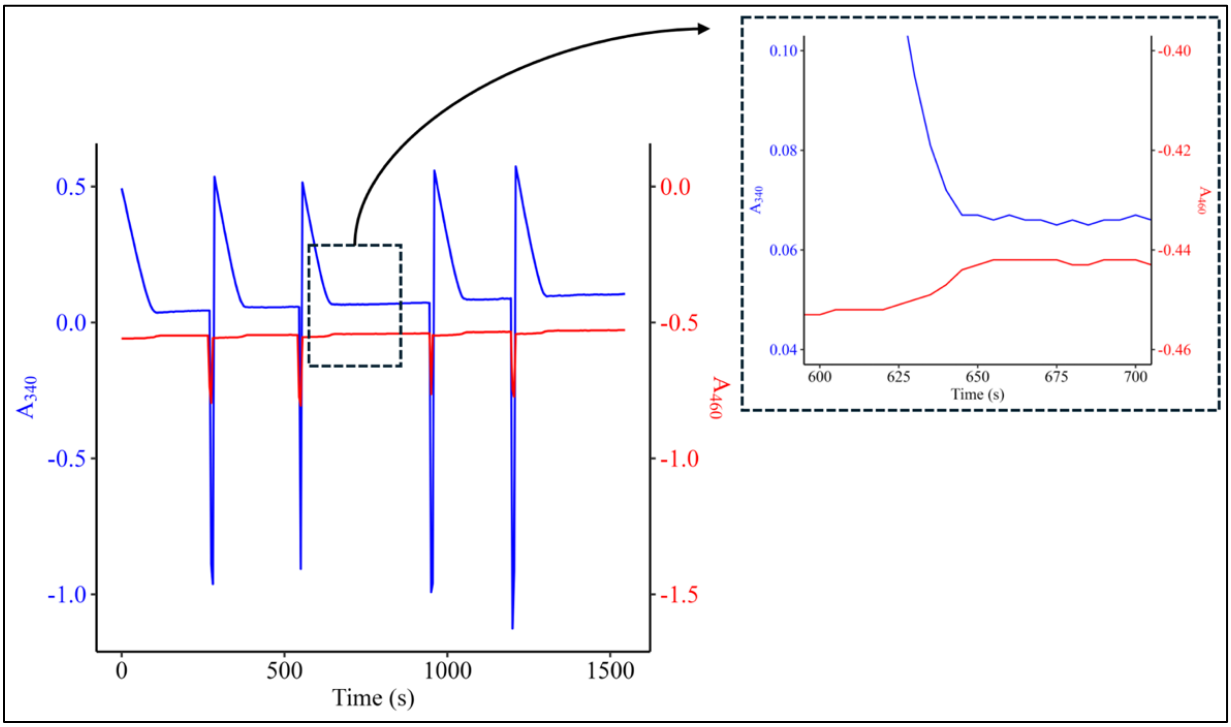

Figure 26: HRP/ODA assay where the decrease in NADH (A_{340}, blue) and the increase in red colour of ODA (A_{460}, red) were measured simultaneously on the spectrophotometer. Cuvette contained 1 µM FAD, 1 µM gFlHb, 0.475 U/mL HRP, and 0.1 mg/mL ODA in 100 mM Bis-Tris buffer (pH 6.5). Reaction was maintained at 37ºC and five additions of 100 µM NADH were made to initiate the reactions.

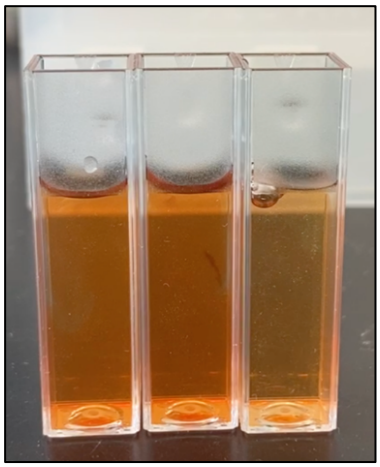

Figure 27: NADH interference with the HRP/ODA assay. All cuvettes contain 0.475 U/mL HRP, 0.1 mg/mL ODA, and 100 µM hydrogen peroxide in 100 mM Bis-Tris buffer (pH 6.5). 1 µM gFlHb, 1 µM FAD, and 100 µM NADH were added to the left, middle, and right cuvettes, respectively.

The free radical analyzer equipped with a hydrogen peroxide sensing electrode confirmed hydrogen peroxide production by gFlHb under aerobic conditions, with generation occurring only when NADH was present (Figure 28). The addition of catalase brought the hydrogen peroxide levels back down to the baseline. Based on this reaction, approximately 40 µM hydrogen peroxide was generated.

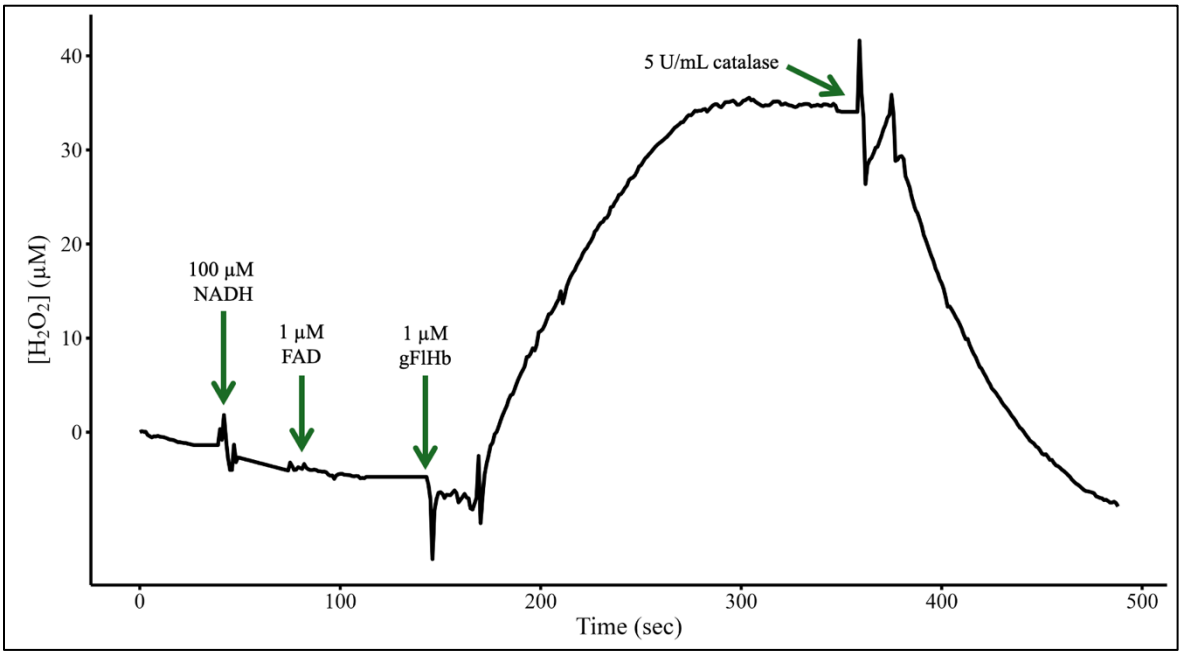

Figure 28: Free radical analyzer HPO kinetic trace. Current changes were converted to hydrogen peroxide concentrations via calibration curve (Figure A1). Where indicated, 100 µM NADH, 1 µM FAD, 1 µM gFlHb, 5 U/mL catalase were added.

In addition to its generation, hydrogen peroxide was found to degrade the heme group of Hmp and gFlHb in concentration-dependent manners (Figure 29, 30). The observed decrease in heme absorbance following peroxide addition was greater in gFlHb compared to Hmp over time, indicating that gFlHb may be more susceptible to oxidative damage (Figure 31). Endogenous hydrogen peroxide generated during the NADH oxidase reaction also contributed to heme degradation in gFlHb, as shown by the progressive loss of heme absorbance over time (Figure 32). This degradation pattern closely mirrored the

effects of exogenous hydrogen peroxide addition, implying that gFlHb may undergo self-inflicted oxidative damage. Interestingly, while Hmp is more resistant to hydrogen peroxide, it instead produces superoxide anions as a self-destruction mechanism.[82] To support this, in the absence of its substrate, L-arginine, nitric oxide synthases generate superoxide.[83–85] A similar substrate-dependent shift may occur in gFlHb where in the absence of nitric oxide, it produces hydrogen peroxide as a self-regulatory mechanism. This could serve as a means of energy conservation, preventing unnecessary NADH consumption and resource depletion, or as a protective mechanism to limit reactive oxygen species formation.

Further studies should investigate whether gFlHb can consume hydrogen peroxide under anaerobic conditions, similar to Hmp. If this were the case, it would be important to determine whether a threshold exists where sufficient oxygen is consumed to generate hydrogen peroxide aerobically, creating an environment anaerobic enough to promote its subsequent consumption. Since this activity has only been studied in the absence of nitric oxide, future experiments should include the addition of nitric oxide donors to assess whether hydrogen peroxide generation is entirely supressed when the primary substrate for flavohemoglobins is present. To determine the role the heme group plays in hydrogen peroxide generation, addition of strong inhibitors like sodium cyanide should be explored. Finally, the effect of cytochrome *c*, an alternative electron acceptor should be explored. In NADH oxidase assays, adding cytochrome *c* increased the rate of absorbance decrease at 340 nm, as electrons had two potential pathways: oxygen or cytochrome *c*. However, in this context, cytochrome *c* is expected to divert electrons away from oxygen, thereby preventing its reduction and limiting hydrogen peroxide formation, ultimately decreasing the observed activity.

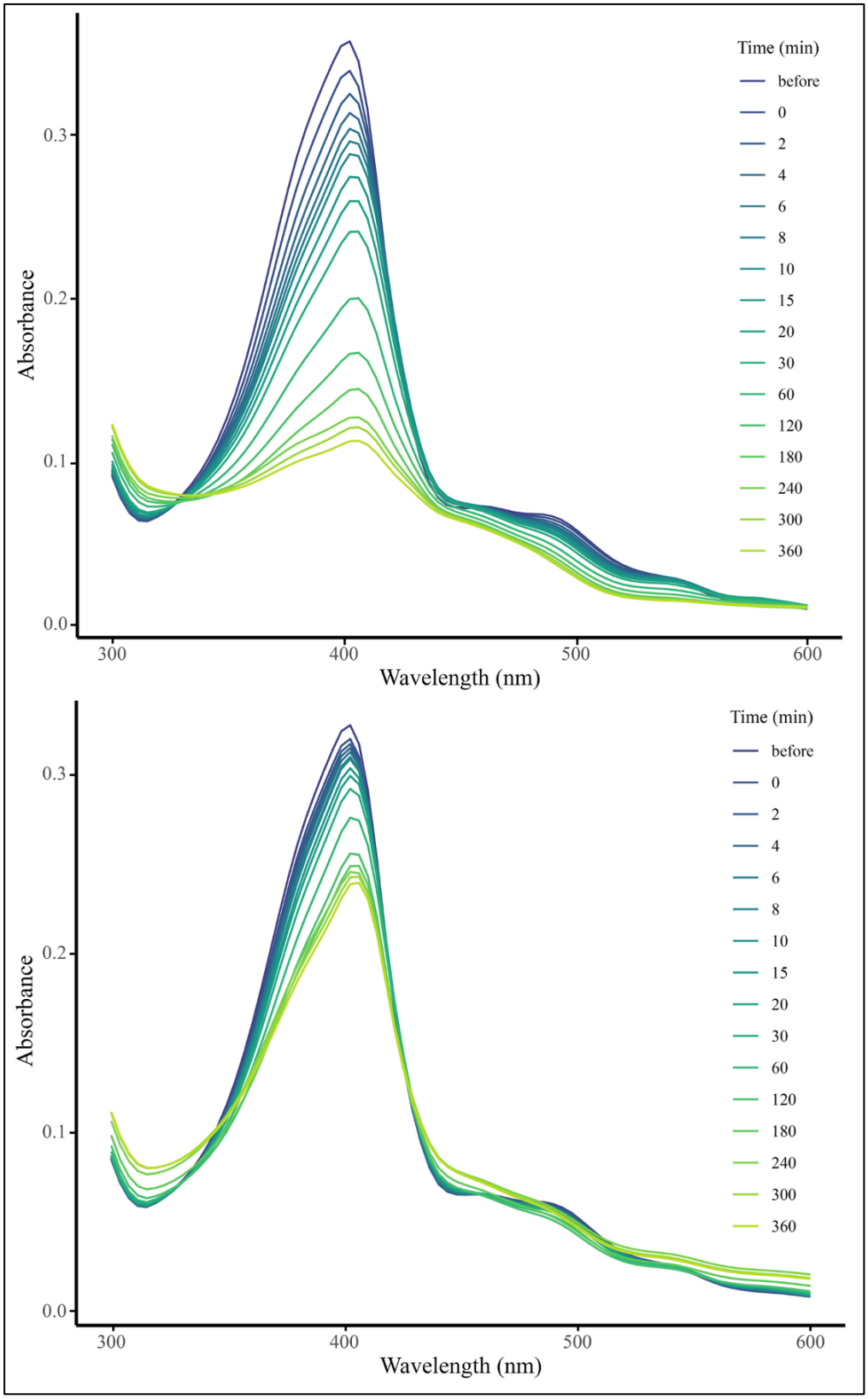

Figure 29: Hmp heme breakdown over time in the presence of 0.5 mM H_2O_2 (top) and 0.1 mM H_2O_2 (bottom), represented by the decrease in absorbance of the Soret peak.

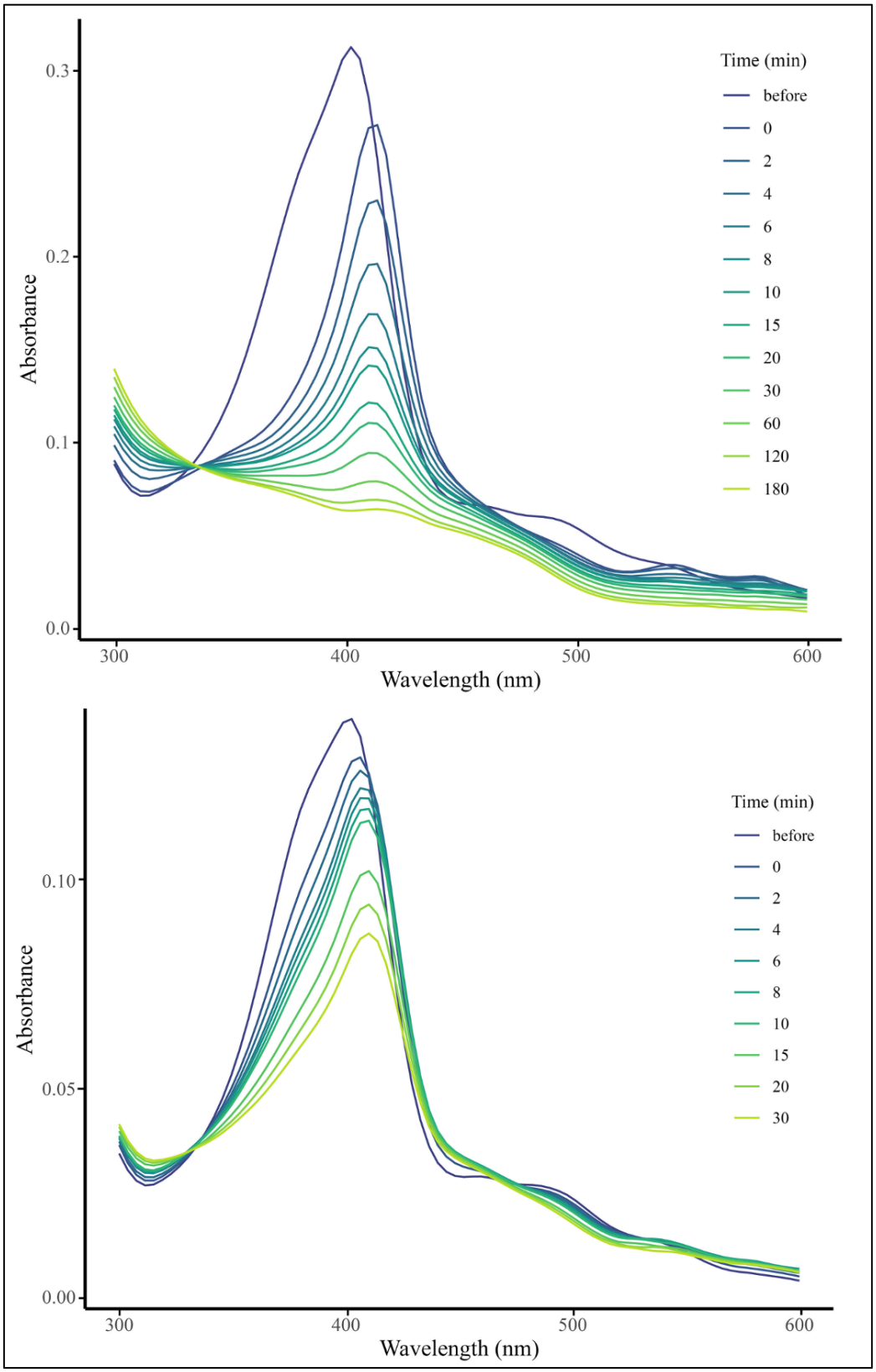

Figure 30: gFlHb heme breakdown over time with 0.5 mM H_2O_2 on two different protein preparations.

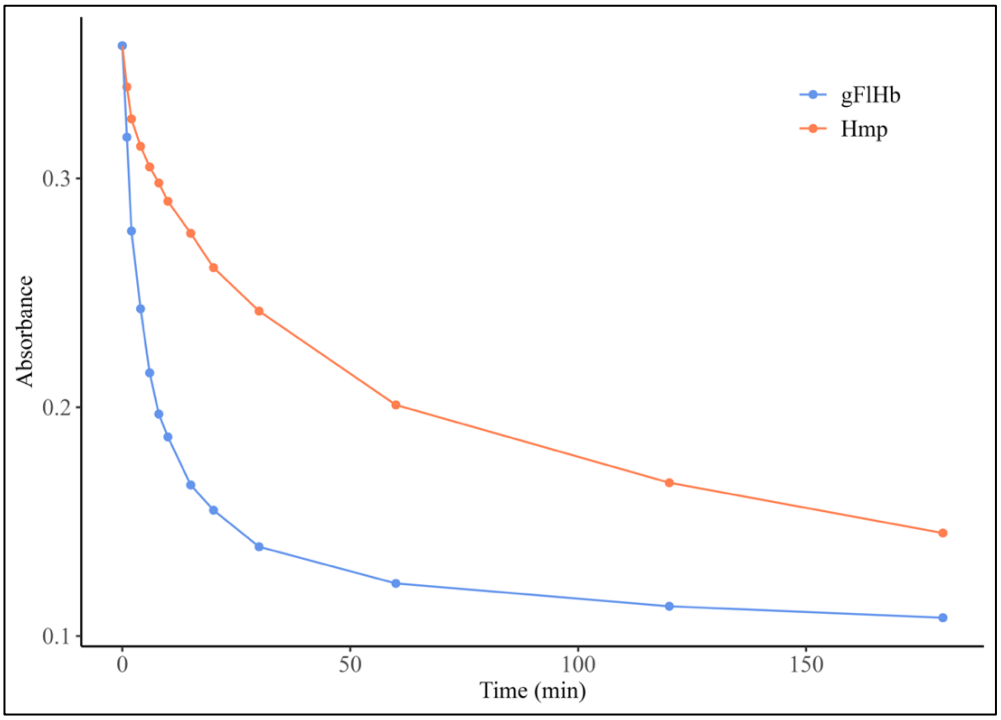

Figure 31: Absorbance changes in the Soret peak for gFlHb (blue) and Hmp (orange) over time following 0.5 µM hydrogen peroxide addition. The gFlHb data was adjusted by adding 0.044 absorbance units to align initial readings for comparison with Hmp.

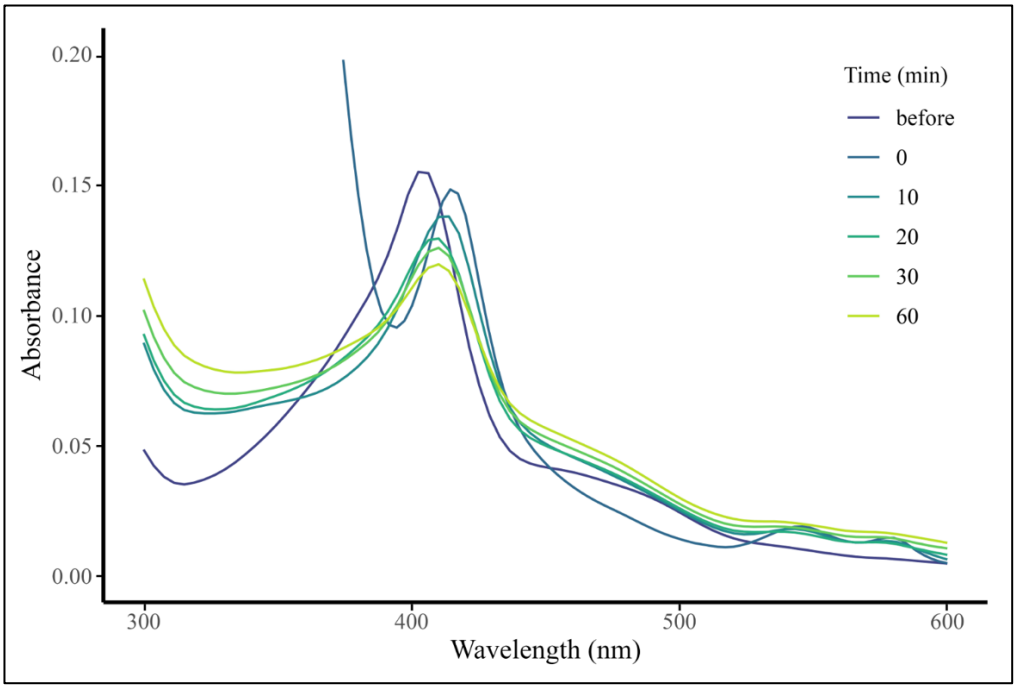

Figure 32: gFlHb heme breakdown over time from endogenously produced hydrogen peroxide. Based on simultaneous measurements on the free radical analyzer, 100 µM hydrogen peroxide was formed.

3.6. Future directions

Collectively, these experiments contribute to the existing knowledge of gFlHb, highlighting critical gaps regarding the significance of its NADH oxidase activity and its role in oxidative stress. Future studies should further investigate the functional importance of the sequence inserts in gFlHb. While we predict that these inserts contribute to protein stability, this remains to be confirmed. Examining more mutants, deleting these inserts entirely, and assessing the thermostability of the resulting mutant proteins will provide valuable insights into their role.

Additionally, metronidazole-resistant Giardia strains harbour conserved mutations within the gFlHb gene, suggesting a potential link between gFlHb and drug susceptibility. Notably, more than half of these mutations localize to the sequence inserts.[48] Although gFlHb copy number does not directly influence metronidazole resistance,[86] characterizing the functional impact of gFlHb variants carrying these mutations may offer valuable insights into the role of the sequence inserts in maintaining protein function and their possible involvement in metronidazole resistance.

Identification of an inhibitor as potent as cyanide while avoiding its toxicity would be a substantial discovery in drug development for giardiasis. While gFlHb has not yet been confirmed as a viable drug target due to challenges in gene knockouts, identifying inhibitors of this protein remains a promising avenue. Future research should explore the impact of isocyanide compounds, such as Xanthocillin, on flavohemoglobin activity.

The role of flavohemoglobin-associated lipids also remains unresolved. Current experiments indicate that lipids bind to gFlHb, but their functional significance is unclear. To address this, future studies should focus on optimizing lipid-removal techniques and

measuring NADH oxidase activity before and after lipid removal to determine their influence on enzyme function.

Finally, further characterization of gFlHb's newly proposed activity requires measuring the rate of hydrogen peroxide generation by gFlHb and NADH in the presence of nitric oxide, gFlHb's primary substrate, as well as cytochrome *c*, a potential alternative electron acceptor. Additionally, recreating the anaerobic conditions under which Hmp breaks down peroxide could reveal whether gFlHb exhibits similar behaviour. Identifying the switching point between peroxide buildup and breakdown would provide significant insight into this potential self-regulatory mechanism.

4. CONCLUSIONS

The differences in NADH oxidase and cytochrome *c* reductase activities between Hmp and gFlHb suggest evolutionary divergence shaped by their respective oxygen environments. Hmp, derived from the more oxygen-tolerant *E. coli*, appears optimized for managing oxidative stress, whereas gFlHb may have adapted to a microaerotolerant niche by minimizing superoxide production. This divergence reveals the need for further structural and functional characterization of gFlHb's unique sequence inserts, which may also contribute to its distinct enzymatic properties. Advanced structural techniques such as cryo-EM or X-ray crystallography could provide crucial insights into how these inserts influence function and stability.

Across *Giardia intestinalis* assemblages A, B, and E, flavohemoglobins exhibit similar NADH oxidase activities but display subtle variations in FAD and NADH dependence. Given their sequence similarities–87% between gFlHb A and E, 71% between gFlHb A and B, and 75% between gFlHb B and E–only minor functional differences were expected. However, potential variations in nitric oxide dioxygenase inhibition among these assemblages could have significant implications for drug development. If assemblage specific differences exist, they may be exploited to design targeted inhibitors. In contrast, the absence of such differences would be advantageous, allowing for broad-spectrum therapeutics that do not require assemblage-specific drugs.

The NADH oxidase activity in gFlHb was not inhibited by imidazole, miconazole, and nitrite, though cyanide caused a decreased in activity. The potency of cyanide may be due to its ability to bind flavohemoglobins in both the oxidized and the reduced-deoxygenated state. These findings suggest that NADH oxidation does not require the

heme group for electron transfer. Instead, the electrons likely follow an alternative path in gFlHb, possibly diverted through FAD towards molecular oxygen, where it can be reduced to superoxide or hydrogen peroxide.

Flavohemoglobin-lipid interactions have been extensively studied in Hmp, though direct translation to gFlHb may not be straightforward. Lipid extracts from gFlHb A, B, and E revealed lipid conservations, with differences primarily in the relative abundance of mass spectrometry peaks. These interactions could potentially influence gFlHb's structural and functional properties. Further characterization, along with attempts to remove lipids, is necessary to better understand their precise role and functional impact.

The parallels between nitric oxide synthases and gFlHb suggest that gFlHb may play a more dynamic role in redox balance than previously recognized. In particular, the protein may engage in a self-regulating feedback loop, modulating its activity in response to nitric oxide availability. This thesis also highlights a previously unappreciated relationship between NADH oxidase activity, hydrogen peroxide generation, and heme degradation in gFlHb. The progressive loss of heme, both in response to exogenous hydrogen peroxide and endogenously generated peroxide, suggests that gFlHb undergoes self-inflicted oxidative damage. This mechanism may serve as an adaptive strategy for Giardia, ensuring that oxidative stress is carefully regulated to balance metabolic demands and environmental challenges.

Overall, these findings reveal a complex interplay between redox-active enzymes in Giardia, providing a foundation for future research into their roles in parasite survival and pathogenesis. Understanding these mechanisms not only deepens our knowledge of Giardia's oxidative stress responses but also presents new avenues for therapeutic intervention.

REFERENCES

(1) Berhe, B.; Mardu, F.; Tesfay, K.; Legese, H.; Adhanom, G.; Haileslasie, H.; Gebremichail, G.; Tesfanchal, B.; Shishay, N.; Negash, H. More than Half Prevalence of Protozoan Parasitic Infections among Diarrheic Outpatients in Eastern Tigrai, Ethiopia, 2019; a Cross-Sectional Study. *Infect. Drug. Resist.* **2020**, *13*, 27–34. https://doi.org/10.2147/IDR.S238493.

(2) Center for Disease Control and Prevention. Giardiasis. CDC.gov. https://www.cdc.gov/dpdx/giardiasis/index.html (accessed 2025-02-19).

(3) Li, J., Wang, Z., Karim, M., Zhang, L. Detection of Human Intestinal Protozoan Parasites in Vegetables and Fruits. *Parasit. Vectors* **2020**, 13 (380). https://doi.org/10.1186/s13071-020-04255-3.

(4) Hooshyar, H.; Rostamkhani, P.; Arbabi, M.; Delavari, M. *Giardia lamblia* Infection: Review of Current Diagnostic Strategies. *Gastroenterol. Hepatol. Bed Bench* **2019**, *12* (1), 3–12.

(5) Halliez, M. C. M.; Buret, A. G. Extra-Intestinal and Long Term Consequences of *Giardia duodenalis* Infections. *World J. Gastroenterol.* **2013**, *19* (47), 8974–8985. https://doi.org/10.3748/wjg.v19.i47.8974.

(6) Farbey, M. D.; Reynoldson, J. A.; Thompson, R. C. A. In Vitro Drug Susceptibility of 29 Isolates of *Giardia duodenalis* from Humans as Assessed by an Adhesion Assay. *Int. J. Parasitol.* **1995**, *25* (5), 593–599. https://doi.org/10.1016/0020-7519(94)00174-m.

(7) Argüello-García, R.; Leitsch, D.; Skinner-Adams, T.; Ortega-Pierres, M. G. Drug Resistance in Giardia: Mechanisms and Alternative Treatments for Giardiasis. In Advances in Parasitology, Vol. 107; Academic Press, 2020; pp 201–282. https://doi.org/10.1016/bs.apar.2019.11.003.

(8) Bernander, R.; Palm, J. E. D.; Svärd, S. G. Genome Ploidy in Different Stages of the *Giardia lamblia* Life Cycle. *Cell. Microbiol.* **2001**, *3* (1), 55–62. https://doi.org/10.1046/j.1462-5822.2001.00094.x.

(9) Lauwaet, T.; Davids, B. J.; Reiner, D. S.; Gillin, F. D. Encystation of *Giardia lamblia*: A Model for Other Parasites. *Curr. Opin. Microbiol.* **2007**, *10* (6), 554–559. https://doi.org/10.1016/j.mib.2007.09.011.

(10) Espey, M. G. Role of Oxygen Gradients in Shaping Redox Relationships between the Human Intestine and Its Microbiota. *Free Radical Biol. Med.* **2013**, *55*, 130–140. https://doi.org/10.1016/j.freeradbiomed.2012.10.554.

(11) Brown, D. M.; Upcroft, J. A.; Edwards, M. R.; Upcroft, P. Anaerobic Bacterial Metabolism in the Ancient Eukaryote *Giardia duodenalis*. *Int. J. Parasitol.* **1998**, *28*, 149–164. https://doi.org/10.1016/s0020-7519(97)00172-0.

(12) Adam, R. D. Biology of *Giardia lamblia*. *Clin. Microbiol. Rev.* **2001**, *14* (3), 447–475. https://doi.org/10.1128/CMR.14.3.447-475.2001.

(13) Bartelt, L. A.; Sartor, R. B. Advances in Understanding Giardia: Determinants and Mechanisms of Chronic Sequelae. *F1000Prime Rep*. **2015**, *7*. https://doi.org/10.12703/P7-62.

(14) Canny, G. O.; McCormick, B. A. Bacteria in the Intestine, Helpful Residents or Enemies from Within? *Infect. Immun.* **2008**, *76* (8), 3360–3373. https://doi.org/10.1128/IAI.00187-08.

(15) Feng, Y.; Xiao, L. Zoonotic Potential and Molecular Epidemiology of Giardia Species and Giardiasis. *Clin. Microbiol. Rev.* **2011**, *24* (1), 110–140. https://doi.org/10.1128/CMR.00033-10.

(16) Cheissin, E. M. Ultrastructure of Lamblia Duodenalis: Body Surface, Sucking Disc, and Median Bodies. *J. Protozool.* **1964**, *11* (1), 91–98. https://doi.org/10.1111/j.1550-7408.1964.tb01725.x.

(17) Friend, D. S. The Fine Structure of *Giardia muris*. *J. Cell Biol.* **1966**, *29*, 317–332. https://doi.org/10.1083/jcb.29.2.317.

(18) Feely, D. E.; Erlandsen, S. L. Morphology of *Giardia agilis*: Observation by Scanning Electron Microscopy and Interference Reflexion Microscopy. *J. Protozool.* **1985**, *32* (4), 691–693. https://doi.org/10.1111/j.1550-7408.1985.tb03103.x.

(19) Kooyman, F. N. J.; Wagenaar, J. A.; Zomer, A. Whole-Genome Sequencing of Dog-Specific Assemblages C and D of *Giardia duodenalis* from Single and Pooled Cysts Indicates Host-Associated Genes. *Microb. Genom.* **2019**, *5* (12). https://doi.org/10.1099/mgen.0.000302.

(20) Marrocco, I.; Altieri, F.; Peluso, I. Measurement and Clinical Significance of Biomarkers of Oxidative Stress in Humans. *Oxid. Med. Cell Longev.* **2017**, *2017*. https://doi.org/10.1155/2017/6501046.

(21) Testa, F.; Mastronicola, D.; Cabelli, D. E.; Bordi, E.; Pucillo, L. P.; Sarti, P.; Saraiva, L. M.; Giuffrè, A.; Teixeira, M. The Superoxide Reductase from the Early Diverging Eukaryote *Giardia intestinalis*. *Free Radical Biol. Med.* **2011**, *51* (8), 1567–1574. https://doi.org/10.1016/j.freeradbiomed.2011.07.017.

(22) Mastronicola, D.; Falabella, M.; Testa, F.; Pucillo, L. P.; Teixeira, M.; Sarti, P.; Saraiva, L. M.; Giuffrè, A. Functional Characterization of Peroxiredoxins from the Human Protozoan Parasite *Giardia intestinalis*. *PLoS Negl. Trop. Dis.* **2014**, *8* (1), e2631. https://doi.org/10.1371/journal.pntd.0002631.

(23) Brown, D. M.; Upcroft, J. A.; Upcroft, P. A H2O-Producing NADH Oxidase from the Protozoan Parasite *Giardia duodenalis*. *Eur. J. Biochem.* **1996**, *241* (1), 155–161. https://doi.org/10.1111/j.1432-1033.1996.0155t.x.

(24) Phaniendra, A.; Jestadi, D. B.; Periyasamy, L. Free Radicals: Properties, Sources, Targets, and Their Implication in Various Diseases. *Indian J. Clin. Biochem.* **2015**, *30* (1), 11–26. https://doi.org/10.1007/s12291-014-0446-0.

(25) Di Matteo, A.; Scandurra, F. M.; Testa, F.; Forte, E.; Sarti, P.; Brunori, M.; Giuffrè, A. The O_2-Scavenging Flavodiiron Protein in the Human Parasite *Giardia intestinalis*. Journal of Biological Chemistry 2008, 283 (7), 4061–4068. https://doi.org/10.1074/jbc.M705605200.

(26) Brown, D. M.; Upcroft, J. A.; Upcroft, P. Free Radical Detoxification in *Giardia duodenalis*. Mol Biochem Parasitol 1995, 72, 47–56. https://doi.org/10.1016/0166-6851(95)00065-9.

(27) Wang, F.; Yuan, Q.; Chen, F.; Pang, J.; Pan, C.; Xu, F.; Chen, Y. Fundamental Mechanisms of the Cell Death Caused by Nitrosative Stress. *Front. Cell Dev. Biol.* **2021**, 9 (742438). https://doi.org/10.3389/fcell.2021.742483.

(28) Rehder, D. Bioinorganic Chemistry; Oxford University Press: Oxford, 2014; pp 115-119.

(29) Li, E.; Zhou, P.; Singer, S. M. Neuronal Nitric Oxide Synthase Is Necessary for Elimination of *Giardia lamblia* Infections in Mice. *J. Immunol.* **2006**, 176, 516–521.

(30) Stadelmann, B.; Hanevik, K.; Andersson, M. K.; Bruserud, O.; Svärd, S. G. The Role of Arginine and Arginine-Metabolizing Enzymes during Giardia-Host Cell Interactions in Vitro. *BMC Microbiol.* **2013**, 13 (256). https://doi.org/10.1186/1471-2180-13-256.

(31) Gardner, P. R.; Gardner, A. M.; Martin, L. A.; Salzman, A. L. Nitric Oxide Dioxygenase: An Enzymic Function for Flavohemoglobin. *PNAS* **1998**, 95, 10378–10383. https://doi.org/10.1073/pnas.95.18.10378.

(32) Poole, R. K.; Ioannidis, N.; Orii, Y. Reactions of the *Escherichia coli* Flavohaemoglobin (Hmp) with NADH and near-Micromolar Oxygen: Oxygen Affinity of NADH Oxidase Activity. *Microbiol.* **1996**, *142*, 1141–1142. https://doi.org/10.1098/rspb.1994.0036.

(33) Rafferty, S.; Luu, B.; March, R. E.; Yee, J. *Giardia lamblia* Encodes a Functional Flavohemoglobin. *Biochem. Biophys. Res. Commun.* **2010**, *399* (3), 347–351. https://doi.org/10.1016/j.bbrc.2010.07.073.

(34) Perutz, M. F.; Kendrew, J. C.; Watson, H. C. Structure and Function of Haemoglobin. *J. Mol. Biol.* **1965**, *13*, 669–678. https://doi.org/10.1016/S0022-2836(65)80134-6.

(35) Rafferty, S. P.; Dayer, G. Heme Proteins of *Giardia intestinalis*. *Exp. Parasitol.* **2015**, *159*, 13–23. https://doi.org/10.1016/j.exppara.2015.08.001.

(36) Mukai, M.; Mills, C. E.; Poole, R. K.; Yeh, S. R. Flavohemoglobin, a Globin with a Peroxidase-like Catalytic Site. *J. Biol. Chem.* **2001**, *276* (10), 7272–7277. https://doi.org/10.1074/jbc.M009280200.

(37) Ollesch, G.; Kaunzinger, A.; Juchelka, D.; Schubert-Zsilavecz, M.; Ermler, U. Phospholipid Bound to the Flavohemoprotein from *Alcaligenes eutrophus*. *Eur. J. Biochem.* **1999**, *262*, 396–405. https://doi.org/10.1046/j.1432-1327.1999.00381.x.

(38) Milani, M.; Pesce, A.; Ouellet, H.; Guertin, M.; Bolognesi, M. Truncated Hemoglobins and Nitric Oxide Action. *IUBMB Life* 2003, *55* (10–11), 623–627. https://doi.org/10.1080/15216540310001628708.

(39) El Hammi, E.; Warkentin, E.; Demmer, U.; Limam, F.; Marzouki, N. M.; Ermler, U.; Baciou, L. Structure of *Ralstonia eutropha* Flavohemoglobin in Complex with Three Antibiotic Azole Compounds. *Biochemistry* **2011**, *50* (7), 1255–1264. https://doi.org/10.1021/bi101650q.

(40) Ilari, A.; Bonamore, A.; Farina, A.; Johnson, K. A.; Boffi, A. The X-Ray Structure of Ferric *Escherichia coli* Flavohemoglobin Reveals an Unexpected Geometry of the Distal Heme Pocket. *J. Biol. Chem.* **2002**, *277* (26), 23725–23732. https://doi.org/10.1074/jbc.M202228200.

(41) Helmick, R. A.; Fletcher, A. E.; Gardner, A. M.; Gessner, C. R.; Hvitved, A. N.; Gustin, M. C.; Gardner, P. R. Imidazole Antibiotics Inhibit the Nitric Oxide Dioxygenase Function of Microbial Flavohemoglobin. *Antimicrob. Agents Chemother*. **2005**, *49* (5), 1837–1843. https://doi.org/10.1128/AAC.49.5.1837-1843.2005.

(42) Pech-Santiago, E. O.; Argüello-García, R.; Arce-Cruz, G.; Angeles, E.; Ortega-Pierres, G. *Giardia duodenalis* Flavohemoglobin Is a Target of 5-Nitroheterocycle and Benzimidazole Compounds Acting as Enzymatic Inhibitors or Subversive Substrates. *Free Radical Biol. Med.* **2025**, 227, 355–366. https://doi.org/10.1016/j.freeradbiomed.2024.12.020.

(43) Bonamore, A.; Farina, A.; Gattoni, M.; Schininà, M. E.; Bellelli, A.; Boffi, A. Interaction with Membrane Lipids and Heme Ligand Binding Properties of *Escherichia coli* Flavohemoglobin. *Biochem.* **2003**, *42* (19), 5792–5801. https://doi.org/10.1021/bi0206311.

(44) Wisecaver, J. H.; Alexander, W. G.; King, S. B.; Todd Hittinger, C.; Rokas, A. Dynamic Evolution of Nitric Oxide Detoxifying Flavohemoglobins, a Family of Single-Protein Metabolic Modules in Bacteria and Eukaryotes. *Mol. Biol. Evol.* **2016**, *33* (8), 1979–1987. https://doi.org/10.1093/molbev/msw073.

(45) Vasudevan, S. G.; Armarego, W. L.; Shaw, D. C.; Lilley, P. E.; Dixon, N. E.; Poole, R. K. Isolation and Nucleotide Sequence of the Hmp Gene That Encodes a Haemoglobin-like Protein in *Escherichia coli* K-12. *Mol. Gen. Genet.* **1991**, *226*, 49–58. https://doi.org/10.1007/bf00273586.

(46) Xu, F.; Jiménez-González, A.; Einarsson, E.; Ástvaldsson, Á.; Peirasmaki, D.; Eckmann, L.; Andersson, J. O.; Svärd, S. G.; Jerlström-Hultqvist, J. The Compact Genome of *Giardia muris* Reveals Important Steps in the Evolution of Intestinal Protozoan Parasites. *Microb. Genom.* **2020**, *6* (8), 1–15. https://doi.org/10.1099/mgen.0.000402.

(47) Poole, R. K.; Anjum, M. F.; Membrillo-Herna´ndez, J.; Herna´ndez, H.; Kim, S. O.; Hughes, M. N.; Stewart, V. Nitric Oxide, Nitrite, and Fnr Regulation of Hmp (Flavohemoglobin) Gene Expression in *Escherichia coli* K-12. *J. Bacteriol.* **1996**, *178* (18), 5487–5492. https://doi.org/10.1128/jb.178.18.5487-5492.1996.

(48) Saghaug, C. S.; Klotz, C.; Kallio, J. P.; Aebischer, T.; Langeland, N.; Hanevik, K. Genetic Diversity of the Flavohemoprotein Gene of *Giardia lamblia*: Evidence for High Allelic Heterozygosity and Copy Number Variation. *Infect. Drug Resist.* **2020**, *13*, 4531–4545. https://doi.org/10.2147/IDR.S274543.

(49) Andersson, J. O.; Sa, A.; Sjö Gren, M.; Davis, L. A. M.; Martin Embley, T.; Roger, A. J. Phylogenetic Analyses of Diplomonad Genes Reveal Frequent Lateral Gene Transfers Affecting Eukaryotes. *Curr. Biol.* **2003**, *13*, 94–104. https://doi.org/10.1016/s0960-9822(03)00003-4.

(50) Ma'ayeh, S. Y.; Knörr, L.; Svärd, S. G. Transcriptional Profiling of *Giardia intestinalis* in Response to Oxidative Stress. *Int. J. Parasitol.* **2015**, *45* (14), 925–938. https://doi.org/10.1016/j.ijpara.2015.07.005.

(51) Bonamore, A.; Gentili, P.; Ilari, A.; Schininà, M. E.; Boffi, A. *Escherichia coli* Flavohemoglobin Is an Efficient Alkylhydroperoxide Reductase. *J. Biol. Chem.* 2003, 278 (25), 22272–22277. https://doi.org/10.1074/jbc.M301285200.

(52) Membrillo-Hernández, J.; Ioannidis, N.; Poole, R. K. The Flavohaemoglobin (HMP) of *Escherichia coli* Generates Superoxide in Vitro and Causes Oxidative Stress in Vivo. *FEBS Lett*. **1996**, *382* (1–2), 141–144. https://doi.org/10.1016/0014-5793(96)00154-8.

(53) Membrillo-Hernández, J.; Coopamah, M. D.; Anjum, M. F.; Stevanin, T. M.; Kelly, A.; Hughes, M. N.; Poole, R. K. The Flavohemoglobin of *Escherichia coli* Confers Resistance to a Nitrosating Agent, a "Nitric Oxide Releaser," and Paraquat and Is Essential for Transcriptional Responses to Oxidative Stress. *J. Biol. Chem.* **1999**, *274* (2), 748–754. https://doi.org/10.1074/jbc.274.2.748.

(54) Lukaszewicz, B.; McColl, E.; Yee, J.; Rafferty, S.; Couture, M. Resonance Raman Studies on the Flavohemoglobin of the Protist *Giardia intestinalis*: Evidence of a Type I/II-Peroxidase-like Heme Environment and Roles of the Active Site Distal Residues. *J. Biol. Inorg. Chem.* **2017**, *22* (7), 1099–1108. https://doi.org/10.1007/s00775-017-1487-7.

(55) New England Biolabs. Transformation Protocol BL21(DE3).

(56) Mastronicola, D.; Testa, F.; Forte, E.; Bordi, E.; Pucillo, L. P.; Sarti, P.; Giuffrè, A. Flavohemoglobin and Nitric Oxide Detoxification in the Human Protozoan Parasite *Giardia intestinalis*. *Biochem. Biophys. Res. Commun.* **2010**, *399* (4), 654–658. https://doi.org/10.1016/j.bbrc.2010.07.137.

(57) Gardner, P. R.; Gardner, A. M.; Martin, L. A.; Dou, Y.; Li, T.; Olson, J. S.; Zhu, H.; Riggs, A. F. Nitric-Oxide Dioxygenase Activity and Function of Flavohemoglobins. *J. Biol. Chem.* **2000**, *275* (41), 31581–31587. https://doi.org/10.1074/jbc.M004141200.

(58) Wang, C.; Liu, C.; Zhu, X.; Peng, Q.; Ma, Q. Catalytic Site Flexibility Facilitates the Substrate and Catalytic Promiscuity of Vibrio Dual Lipase/Transferase. *Nat. Commun.* **2023**, *14* (1). https://doi.org/10.1038/s41467-023-40455-y.

(59) Hill, S.; Decorso, I.; Nezamololama, N.; Babaei, Z.; Rafferty, S. P. Catalytic Differences between Flavohemoglobins of *Giardia intestinalis* and *E. coli*. *Pathogens* **2024**, *13* (6). https://doi.org/10.3390/pathogens13060480.

(60) Valley, C. C.; Cembran, A.; Perlmutter, J. D.; Lewis, A. K.; Labello, N. P.; Gao, J.; Sachs, J. N. The Methionine-Aromatic Motif Plays a Unique Role in Stabilizing Protein Structure. *J. Biol. Chem.* **2012**, *287* (42), 34979–34991. https://doi.org/10.1074/jbc.M112.374504.

(61) Kuss-Petermann, M.; Wenger, O. S. Electron Transfer Rate Maxima at Large Donor-Acceptor Distances. *J. Am. Chem. Soc.* **2016**, *138* (4), 1349–1358. https://doi.org/10.1021/jacs.5b11953.

(62) Hausladen, A.; Gow, A.; Stamler, J. S. Flavohemoglobin Denitrosylase Catalyzes the Reaction of a Nitroxyl Equivalent with Molecular Oxygen. *PNAS* **2001**, *98* (18), 10108–10112.

(63) Xu, Q.; Qiao, Q.; Gao, Y.; Hou, J.; Hu, M.; Du, Y.; Zhao, K.; Li, X. Gut Microbiota and Their Role in Health and Metabolic Disease of Dairy Cow. *Front. Nutr.* **2021**, *8* (701511). https://doi.org/10.3389/fnut.2021.701511.

(64) Mishra, B.; Jha, R. Oxidative Stress in the Poultry Gut: Potential Challenges and Interventions. *Front. Vet. Sci.* **2019**, *6* (60). https://doi.org/10.3389/fvets.2019.00060.

(65) Novin Nezamololama. Ligand Binding Properties of Giardia Flavohemoglobin, Trent University, Peterborough, **2019**.

(66) Cox, R.; Hollaway, M. The Reduction by Dithionite of Fe (III) Myoglobin Derivatives with Different Ligands Attached to the Iron Atom. *Eur. J. Biochem.* **1977**, 74, 575-587. https://doi.org/10.1111/j.1432-1033.1977.tb11427.x

(67) Yoshikawa, S.; Caugheys, W. Infrared Evidence of Cyanide Binding to Iron and Copper Sites in Bovine Heart Cytochrome *c* Oxidase. *J. Biol. Chem.* **1990**, 265 (14), 7945-7958.

(68) Bellelli, A.; Antonini, G.; Brunori, M.; Springer, B.; Sligar, S. Transient Spectroscopy of the Reaction of Cyanide with Ferrous Myoglobin. *J. Biol. Chem.* **1990**, 265 (31), 18898-18901.

(69) West, A.; Woo, C. Ironing out New Antibiotic Mechanisms with Xanthocillin X. *ACS Cent. Sci.* **2021**, 7 (3), 403-405. https://doi.org/10.1021/acscentsci.1c00130.

(70) Hubner, I.; Shapiro, J.; Hobmann, J.; Drechsel, J.; Hacker, S.; Rather, P.; Pieper, D.; Wuest, W.; Sieber, S. Broad Spectrum Antibiotic Xanthocillin X Effectively Kills *Acinetobacter baumannii* via Dysregulation of Heme Biosynthesis. *ACS Cent. Sci.* **2021**, 7 (3), 488-498. https://doi.org/10.1021/acscentsci.0c01621.

(71) Jan, Y.; Richardson, J.; Baker, A.; Mishin, V.; Heck, D.; Laskin, D.; Laskin, J. Vitamin K3 (menadione) Redox Cycling Inhibits Cytochrome P450-mediated Metabolism and Inhibits Parathion Intoxication. *Toxicol. Appl. Pharmacol.* **2015**, 288 (1), 114-120. https://doi.org/10.1016/j.taap.2015.07.023.

(72) Bag, N.; Wagenknecht-Wiesner, A.; Lee, A.; Shi, S. M.; Holowka, D. A.; Baird, B. A. Lipid-Based and Protein-Based Interactions Synergize Transmembrane Signaling Stimulated by Antigen Clustering of IgE Receptors. *PNAS* **2021**, *118* (35). https://doi.org/10.1073/pnas.2026583118/-/DCSupplemental.

(73) Inuki, S.; Aiba, T.; Hirata, N.; Ichihara, O.; Yoshidome, D.; Kita, S.; Maenaka, K.; Fukase, K.; Fujimoto, Y. Isolated Polar Amino Acid Residues Modulate Lipid Binding in the Large Hydrophobic Cavity of CD1d. *ACS Chem. Biol.* **2016**, *11* (11), 3132–3139. https://doi.org/10.1021/acschembio.6b00674.

(74) Bonamore, A.; Chiancone, E.; Bo, A. The Distal Heme Pocket of *Escherichia coli* Flavohemoglobin Probed by Infrared Spectroscopy. *Biochim. Biophys. Acta* **2001**, *1549*, 174–178. https://doi.org/10.1016/s0167-4838(01)00256-4.

(75) D'Angelo, P.; Lucarelli, D.; Della Longa, S.; Benfatto, M.; Hazemann, J. L.; Feis, A.; Smulevich, G.; Ilari, A.; Bonamore, A.; Boffi, A. Unusual Heme Iron-Lipid Acyl Chain Coordination in Escherichia Coli Flavohemoglobin. *Biophys. J.* **2004**, *86* (6), 3882–3892. https://doi.org/10.1529/biophysj.103.034876.

(76) Kerwin, J. L.; Wiens, A. M.; Ericsson, L. H. Identification of Fatty Acids by Electrospray Mass Spectrometry and Tandem Mass Spectrometry. *J. Mass. Spectrom.* **1996**, *31*, 184–192. https://doi.org/10.1002/(sici)1096-9888(199602)31:2%3C184::aid-jms283%3E3.0.co;2-2.

(77) Pulfer, M.; Murphy, R. C. Electrospray Mass Spectrometry of Phospholipids. *Mass. Spectrom. Rev.* **2003**, *22* (5), 332–364. https://doi.org/10.1002/mas.10061.

(78) Jarroll, E. L.; Muller, P. J.; Meyer, E. A.; Morse, S. A. Lipid and Carbohydrate Metabolism of *Giardia lamblia*. *Mol. Biochem. Parasitol.* **1981**, *2*, 187–196. https://doi.org/10.1016/0166-6851(81)90099-2.

(79) Yu, C.; Li, M.; Sun, Y.; Wang, X.; Chen, Y. Phosphatidylethanolamine Deficiency Impairs *Escherichia coli* Adhesion by Downregulating Lipopolysaccharide Synthesis, Which Is Reversible by High Galactose/Lactose Cultivation. *Cell Commun. Adhes.* **2017**, *23* (1), 1–10. https://doi.org/10.1080/15419061.2017.1282468.

(80) Woodcroft, M.; Ellis, D.; Rafferty, S.; Burns, D.; March, R.; Stock, N.; Trumpour, K.; Yee, J.; Munrok, K. Experimental Characterization of the Mechanism of Perfluorocarboxylic Acids' Liver Protein Bioaccumulation: the Key Role of the Neutral Species. *Environ. Toxicol. Chem.* **2010**, 29 (8), 1669–1677. https://doi.org/10.1002/etc.199.

(81) Seaver, L. C.; Imlay, J. A. Alkyl Hydroperoxide Reductase Is the Primary Scavenger of Endogenous Hydrogen Peroxide in *Escherichia coli*. *J. Bacteriol.* **2001**, *183* (24), 7173–7181. https://doi.org/10.1128/JB.183.24.7173-7181.2001.

(82) Wu, G.; Corker, H.; Orii, Y.; Poole, R. K. *Escherichia coli* Hmp, an "Oxygen-Binding Flavohaemoprotein", Produces Superoxide Anion and Self-Destructs. *Arch. Microbiol.* **2004**, *182* (2–3), 193–203. https://doi.org/10.1007/s00203-004-0699-8.

(83) Pou, S.; Keaton, L.; Surichamorn, W.; Rosen, G. M. Mechanism of Superoxide Generation by Neuronal Nitric-Oxide Synthase. *J. Biol. Chem.* **1999**, *274* (14), 9573–9580. https://doi.org/10.1074/jbc.274.14.9573.

(84) Xia, Y.; Roman, L. J.; Masters, B. S. S.; Zweier, J. L. Inducible Nitric-Oxide Synthase Generates Superoxide from the Reductase Domain. *J. Biol. Chem.* **1998**, *273* (35), 22635–22639. https://doi.org/10.1074/jbc.273.35.22635.

(85) Vasquez-Vivar, J.; Kalyanaraman, B.; Martasek, P.; Hogg, N.; Masters, B. S. S; Karoui, H.; Tordo, P.; Pritchard, K. A. Superoxide Generation by Endothelial Nitric Oxide Synthase: The Influence of Cofactors. *PNAS* **1998**, *95*, 9220–9225.

(86) Korenkova, V.; Weisz, F.; Perglerova, A.; Caccio, S.; Nohynkova, E.; Tumova, P. Comprehensive Analysis of Flavohemoglobin Copy Number Variation in Giardia intestinalis: Exploring Links to Metronidazole Resistance. *Parasit. Vectors*. **2024**, 17 (336). https://doi.org/10.1186/s13071-024-06392-5.

APPENDIX

Table A1: Conserved (black) and non-conserved (red) residues in the NADH-binding and the active site of gFlHb A, B, and E.

Assemblage	Residues in the NADH binding site	Residues in the heme-binding active site
gFlHb A	H246, G321, I322, A351, H353, S382, R399, P425, G427, F428	F25, T26, F29, Y30, M33, L34, L40, I43, F44, H48, Q49, R53, Q54, P55, A57, L58, L59, S61, L62, Y65, Q116, Y117, I119, V120, H123, L124, Y146
gFlHb B	H246, D248, G320, H352, S381, R399, G424, P425, G427, F428, M429, E449, M450, F451	F25, T26, F29, Y30, M33, L34, L40, V43, F44, H48, Q49, R53, Q54, P55, A57, L58, L59, S61, L62, Y65, Q116, Y117, I119, V120, H123, L124, Y146
gFlHb E	H245, G319, A350, A351, H352, S381, R398, P424, G426, F427, A430	F25, T26, F29, Y30, M33, L34, L40, V43, F44, H48, Q49, R53, Q54, P55, A57, L58, L59, S61, L62, Y65, Q115, Y116, I118, V119, H122, L123, Y145

Table A2: Major ESI-MS peaks in the lipid extract of lipid-containing and lipid-free gFlHb B. Lipids were removed from protein samples using lipidex columns.

	Normalization level	
Peaks (m/z)	**gFlHb B**	**'Lipid-free' gFlHb B**
160.8436	1.52E+08	2.65E+08
162.8393	1.47E+08	2.53E+08
164.8462	4.86E+07	8.48E+07
195.8123	1.60E+08	2.11E+08
197.8078	1.87E+08	2.45E+08
199.8071	8.72E+07	1.19E+08
319.0975	5.96E+07	1.26E+08
333.1127	6.20E+07	1.27E+08
365.2509	7.55E+07	9.27E+07
393.2762	7.31E+07	1.03E+08
421.1416	7.95E+07	1.18E+08
449.1736	3.74E+07	5.21E+07
627.5649	3.02E+06	5.82E+06

Table A3: Normalization levels of gFlHb A, B, and E at common m/z ratios measured using negative ESI-MS.

	Normalization level		
Peaks (m/z)	**gFlHb A**	**gFlHb B**	**gFlHb E**
160.84	6.33E+07	1.52E+08	1.48E+08
162.84	5.88E+07	1.47E+08	1.46E+08
164.84	-	4.86E+07	-
195.81	9.27E+07	1.60E+08	1.58E+08
197.81	1.13E+08	1.87E+08	1.89E+08
199.8	5.20E+07	8.72E+07	9.03E+07
319.1	3.76E+07	5.96E+07	1.23E+08
333.11	5.08E+07	6.20E+07	1.47E+08
365.24	1.54E+08	7.55E+07	1.41E+08
393.28	1.84E+08	7.31E+07	1.60E+08
410.22	4.97E+07	-	-
421.14	1.25E+08	7.95E+07	1.02E+08
449.17	7.36E+09	3.74E+07	7.04E+07
519.25	4.05E+07	-	
571.5	3.55E+07	-	
599.52	5.89E+07	-	
627.56	2.76E+07	3.02E+06	6.50E+06
661.44	-	-	2.47E+06
1036.68	1.04E+05	-	
1176.86	-	8.57E+03	
1211.77	-	1.36E+04	3.85E+04

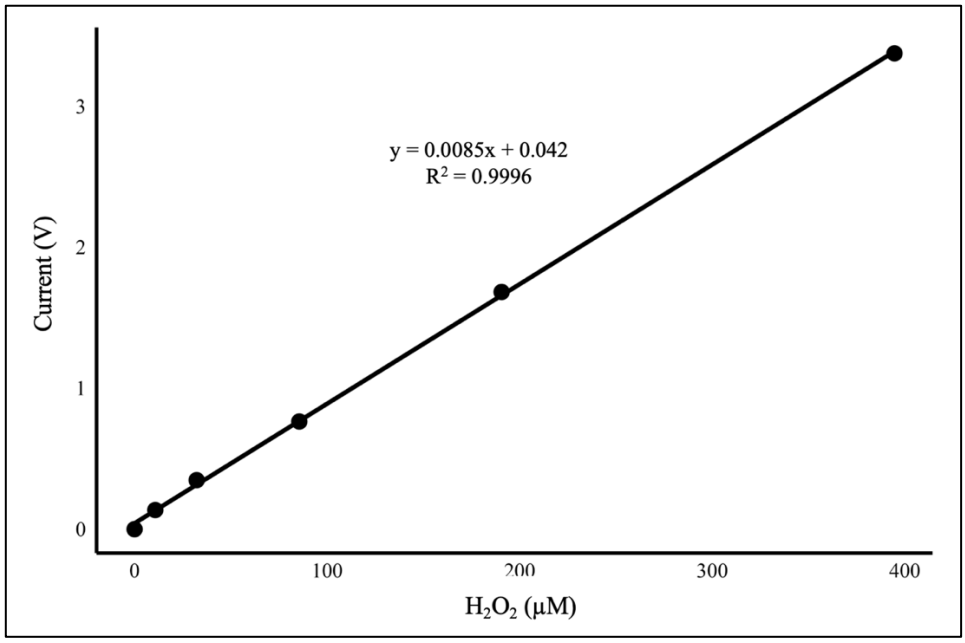

Figure A1: Calibration curve from free radical analyzer converting current changes to hydrogen peroxide concentrations.

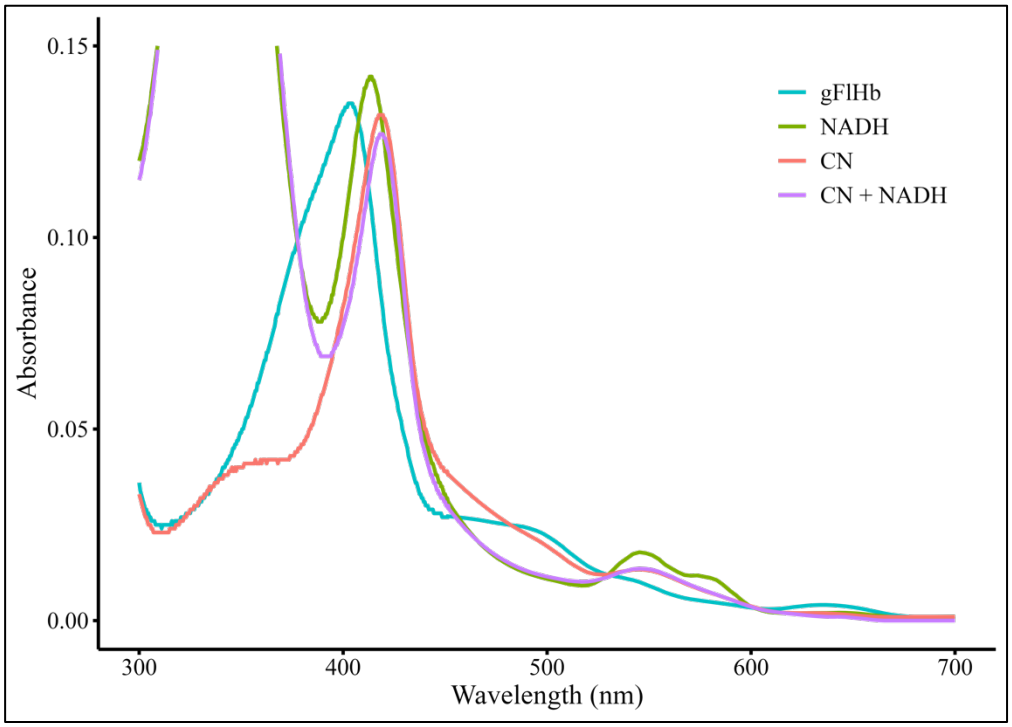

Figure A2: Effects of cyanide on the oxidized (gFlHb; blue) and reduced-oxygenated (NADH; green) states of gFlHb.

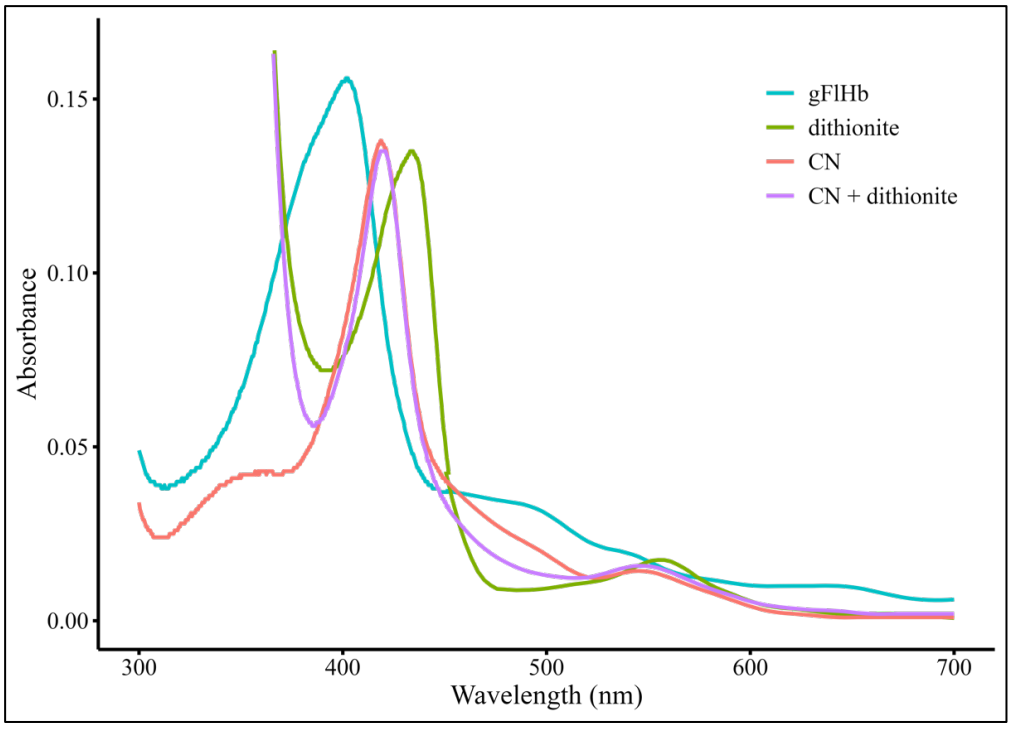

Figure A3: Effects of cyanide on the oxidized (gFlHb; blue) and reduced-deoxygenated (dithionite; green) states of gFlHb.

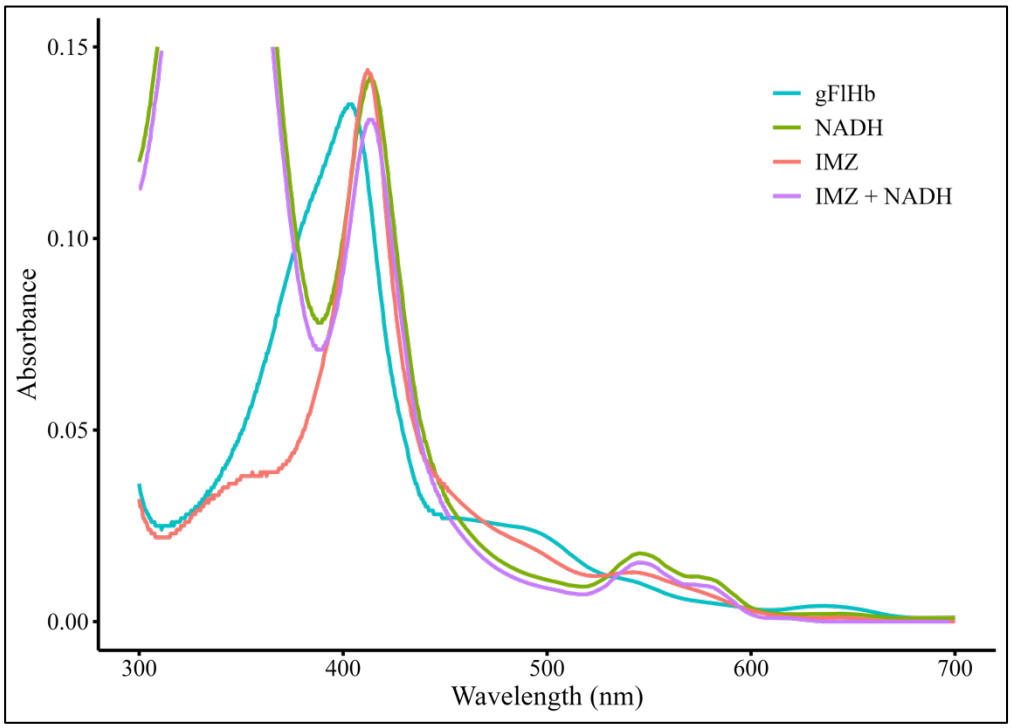

Figure A4: Effects of imidazole (IMZ) on the oxidized (gFlHb; blue) and reduced-oxygenated (NADH; green) states of gFlHb.

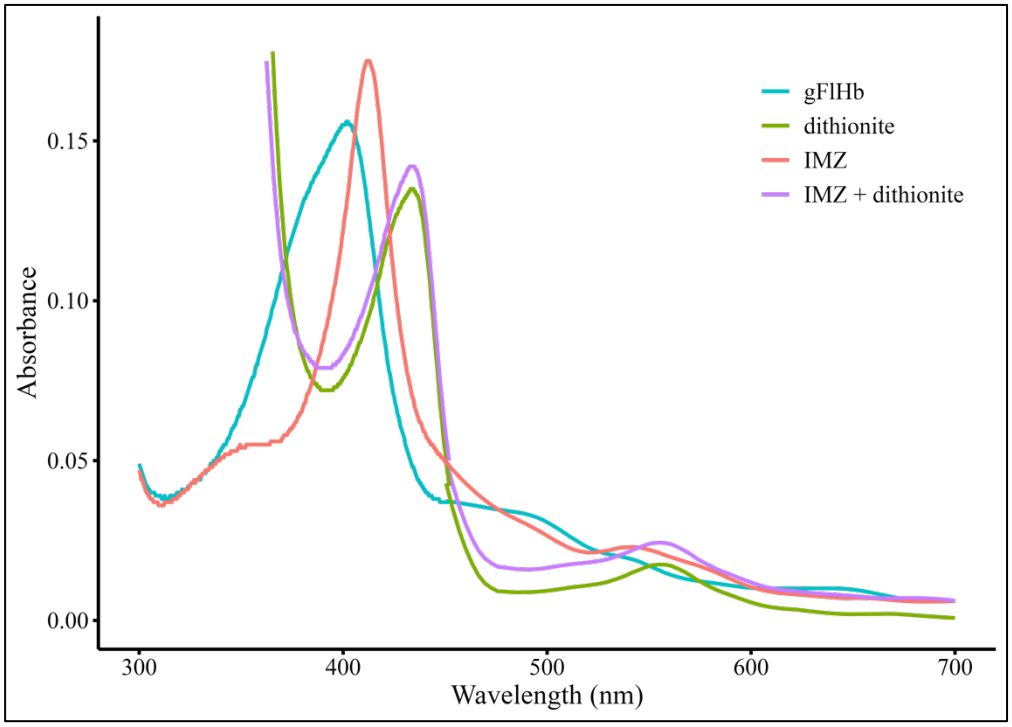

Figure A5: Effects of imidazole (IMZ) on the oxidized (gFlHb; blue) and reduced-deoxygenated (dithionite; green) states of gFlHb.

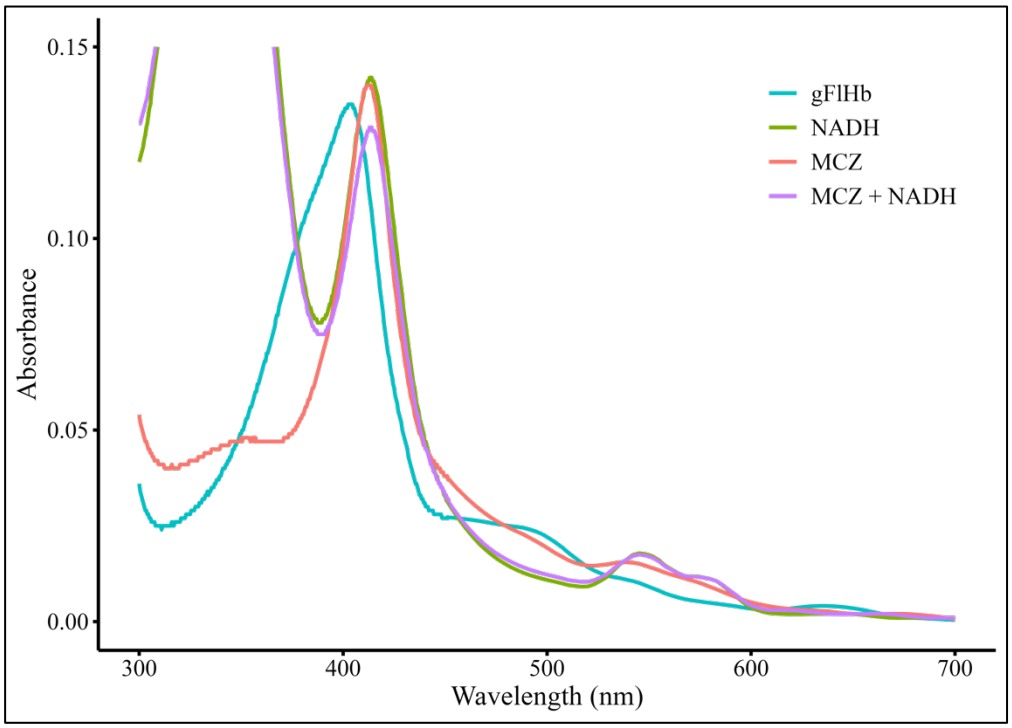

Figure A6: Effects of miconazole (MCZ) on the oxidized (gFlHb; blue) and reduced-oxygenated (NADH; green) states of gFlHb.

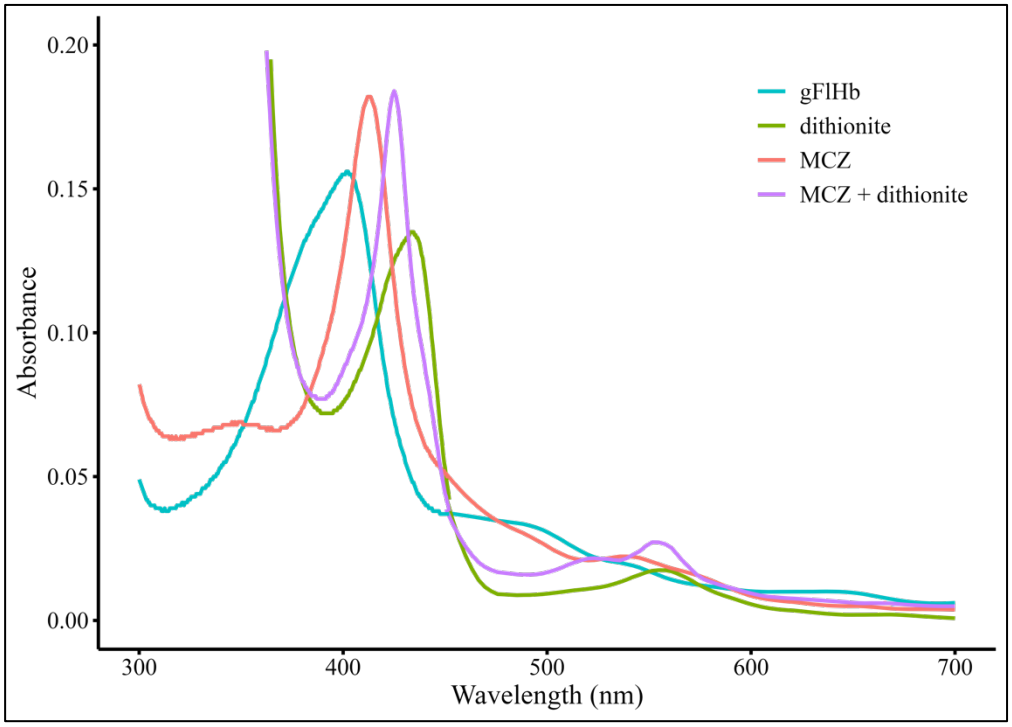

Figure A7: Effects of miconazole (MCZ) on the oxidized (gFlHb; blue) and reduced-deoxygenated (dithionite; green) states of gFlHb.

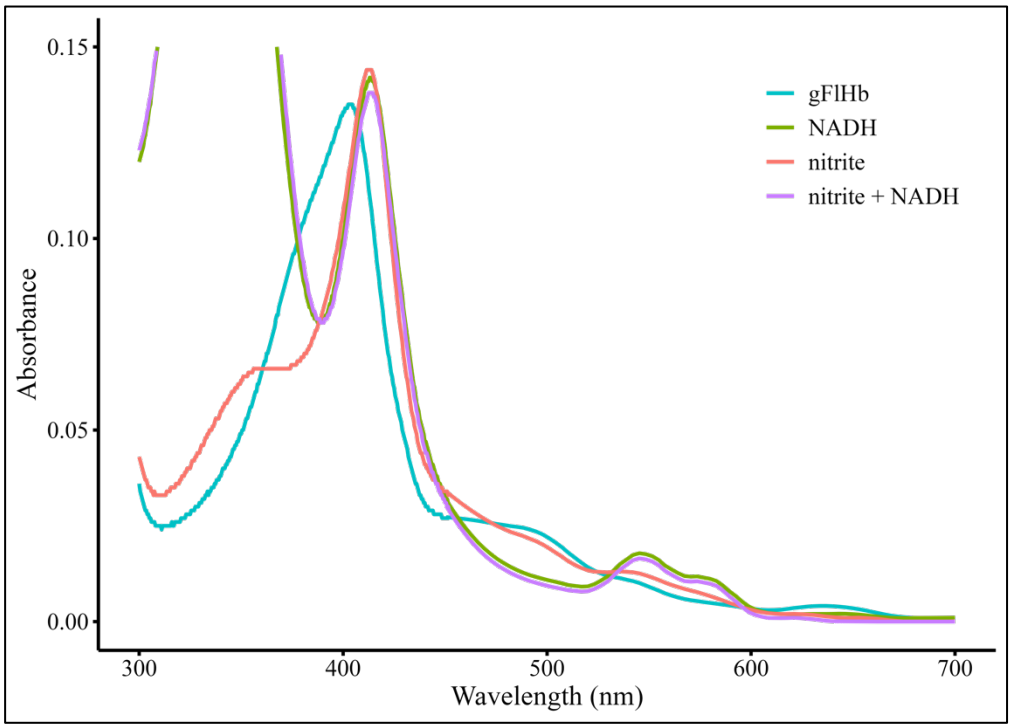

Figure A8: Effects of nitrite on the oxidized (gFlHb; blue) and reduced-oxygenated (NADH; green) states of gFlHb.

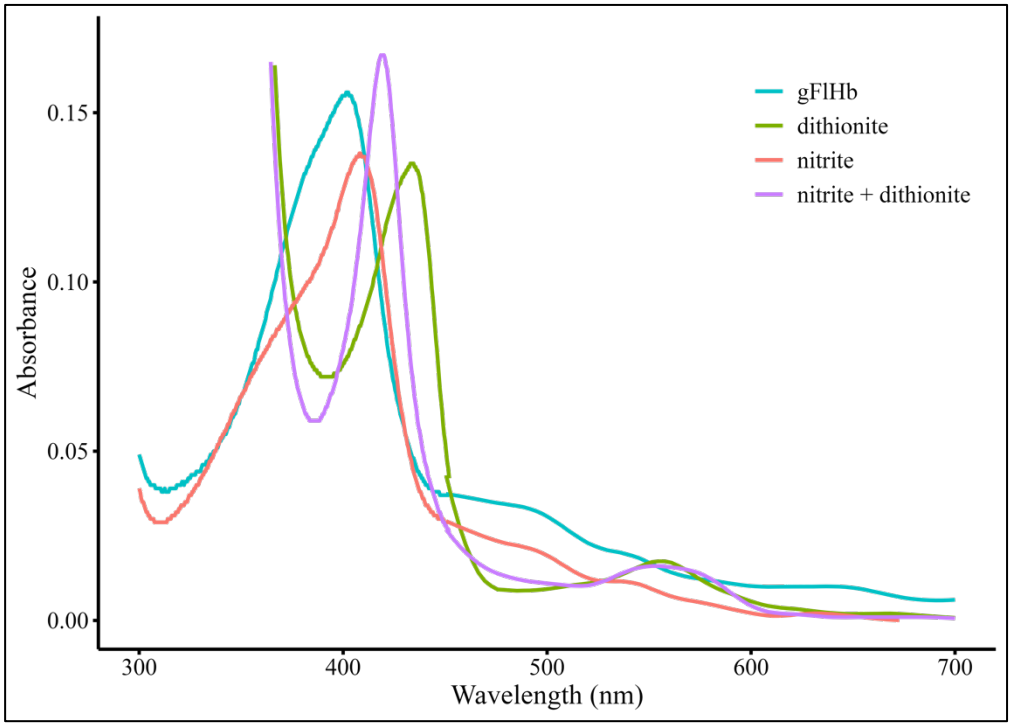

Figure A7: Effects of nitrite on the oxidized (gFlHb; blue) and reduced-deoxygenated (dithionite; green) states of gFlHb.